

**Aerosol simulation
with EMAC**

A. Pozzer et al.

Title Page

Abstract

Introduction

Conclusions

References

Tables

Figures

◀

▶

◀

▶

Back

Close

Full Screen / Esc

Printer-friendly Version

Interactive Discussion



Aerosol simulation applying high resolution anthropogenic emissions with the EMAC chemistry-climate model

A. Pozzer^{1,2}, A. de Meij¹, K. J. Pringle³, H. Tost⁴, U. M. Doering⁵,
J. van Aardenne⁶, and J. Lelieveld^{1,2,7}

¹The Cyprus Institute, Energy, Environment and Water Research Center, P.O. Box 27456, 1645 Nicosia, Cyprus

²Air Chemistry Department, Max-Planck Institute of Chemistry, P.O. Box 3060, 55020 Mainz, Germany

³School of Earth and Environment, Univ. of Leeds, Woodhouse Lane, Leeds, LS2 9JT, UK

⁴Institut für Physik der Atmosphäre, Johannes-Gutenberg Universität Mainz, 55099, Mainz, Germany

⁵Federal Environment Agency (UBA), Wörlitzer Platz 1, 06844, Dessau, Germany

⁶Air and climate change-mitigation, European Environment Agency, Kongens Nytorv 6, 1050 Copenhagen K, Denmark

⁷King Saud University, Riyadh 11451, Saudi Arabia

Received: 5 August 2011 – Accepted: 19 August 2011 – Published: 9 September 2011

Correspondence to: A. Pozzer (pozzer@cyi.ac.cy)

Published by Copernicus Publications on behalf of the European Geosciences Union.

25206

ACPD

11, 25205–25261, 2011

Aerosol simulation with EMAC

A. Pozzer et al.

Title Page

Abstract

Introduction

Conclusions

References

Tables

Figures

⏪

⏩

◀

▶

Back

Close

Full Screen / Esc

Printer-friendly Version

Interactive Discussion



Abstract

The new high resolution global anthropogenic emission inventory (EDGAR-CIRCE) of gas and aerosol pollutants has been incorporated in the chemistry general circulation model EMAC (ECHAM5/MESSy Atmospheric Chemistry). A high horizontal resolution simulation is performed for the years 2005–2008 to evaluate the capability of the model and the emissions to reproduce observed aerosol concentrations and aerosol optical depth (AOD) values. Model output is compared with observations from different measurement networks (CASTNET, EMEP and EANET) and AODs from remote sensing instruments (MODIS and MISR). The model reproduces the main spatial and temporal atmospheric features of the sulfate, ammonium and nitrate aerosol distributions. A good spatial agreement of the distribution of sulfate and ammonium aerosol is found when compared to observations, while calculated nitrate aerosol concentrations show some discrepancies. The simulated temporal development of the inorganic aerosols is in line with measurements of sulfate and nitrate aerosol, while for ammonium aerosol some deviations from observations occur over the USA. The calculated AODs agree well with the satellite observations in most regions, while a negative bias is found for the equatorial area and in the dust outflow regions (i.e. Central Atlantic and Northern Indian Ocean), due to an underestimation of biomass burning and aeolian dust emissions, respectively.

1 Introduction

Tropospheric aerosols have significant effects on human health (Huntingford et al., 2007), the water cycle (Ramanathan et al., 2001) and climate (Isaksen et al., 2009). To study these different topics, global aerosol models that account for a wide range of complexities are required. These models mostly treat five key aerosol species: black carbon (BC), particulate organic carbon (POM), sulfate aerosol (SO_4^{2-}), mineral dust (DU) and sea spray (SS) (see Textor et al., 2006, and reference therein). In recent years, a number of global aerosol models that can treat semi-volatile inorganic species

ACPD

11, 25205–25261, 2011

Aerosol simulation with EMAC

A. Pozzer et al.

Title Page

Abstract

Introduction

Conclusions

References

Tables

Figures

◀

▶

◀

▶

Back

Close

Full Screen / Esc

Printer-friendly Version

Interactive Discussion



**Aerosol simulation
with EMAC**

A. Pozzer et al.

Title Page

Abstract

Introduction

Conclusions

References

Tables

Figures

◀

▶

◀

▶

Back

Close

Full Screen / Esc

Printer-friendly Version

Interactive Discussion



that partition between the gas and aerosol phases have been developed (e.g., Adams et al., 1999; Adams and Seinfeld, 2002; Bauer and Koch, 2005; Myhre et al., 2006; Feng and Penner, 2007; Pringle et al., 2010a). Although models increasingly include sophisticated aerosol descriptions they still rely on offline fields to calculate the emission of precursor gas and many aerosol species. The skill of the aerosol model strongly depends on the representativeness of the emission fields used, thus it is important to consider any possible biases in the emissions. For example, most of the global anthropogenic emissions inventories currently neglect the seasonal cycle of emissions for the majority of precursor gases and generally have a resolution of $1 \times 1^\circ$ (van Aardenne et al., 2005; Olivier et al., 1999, 1996).

The seasonal variation of anthropogenic emissions is important for many compounds (e.g. ammonia) especially for those for which the phase partitioning is temperature dependent (Pinder et al., 2004; De Meij et al., 2006). In this work, we take advantage of the state-of-the-art emissions inventory EDGAR-Climate Change and Impact Research (CIRCE), which provides emissions on a high spatial ($0.1 \times 0.1^\circ$) and temporal (monthly) resolution, together with a recently developed aerosol scheme implemented within the EMAC model (Pringle et al., 2010a).

This study has two main objectives. The first objective is to evaluate the model's performance in simulating gas, aerosol and AODs calculations using the EDGAR-CIRCE emission inventory by comparing the results with ground based and space born observations. The second objective is to analyse the aerosol (precursor) budget for five regions (Europe, North America, East Asia, South America and Central Africa) and quantify the aerosol import and export terms. For this, a relatively high horizontal resolution ($\sim 1 \times 1^\circ$) tropospheric aerosol simulation has been performed and the results have been evaluated against observations. Particular focus is placed on semi-volatile inorganic aerosol species (i.e. SO_4^{2-} , NO_3^- and NH_4^+) and their precursors. A detailed budget analysis is performed, both on a global scale and for different regions, and the results compared with previous studies. Additionally, the effect of including the seasonal cycle in the anthropogenic emissions of aerosol precursors is also investigated.

**Aerosol simulation
with EMAC**

A. Pozzer et al.

Title Page

Abstract

Introduction

Conclusions

References

Tables

Figures

◀

▶

◀

▶

Back

Close

Full Screen / Esc

Printer-friendly Version

Interactive Discussion



The paper is organized as follows. Section 2.1 describes the model, the emission inventory and the observational datasets. In Sect. 3 the evaluation of the aerosol optical depth (AOD) is presented. AOD is a very useful metric for analysing model performance in regions where ground-based observations are sparse. It provides a qualitative indication of the ability of the model to reproduce the concentrations of BC, OC and dust which are often not included in the observational networks. In Sect. 3.2 aerosol concentrations of SO_4^{2-} , NO_3^- and NH_4^+ are compared to large scale observations. Special focus is given to these compounds due to their complex interactions with the gas phase chemistry. Additionally, Na^+ aerosol is also compared to station observations as a proxy for sea salt. To examine the contribution of the different aerosol species to air quality, Sect. 4 shows the global and regional budgets of aerosol in North America, Europe, East Asia, Central Africa and South America. Finally, in Sect. 5 the effects of the seasonally varying anthropogenic emissions are analysed, followed by the conclusion in Sect. 6

2 Model and observations

2.1 Model description and setup

EMAC is a combination of the general circulation model ECHAM5 (Roeckner et al., 2006) (version 5.3.01) and the Modular Earth Submodel System (MESSy, version 1.9, Jöckel et al., 2005). The model has been extensively described and evaluated (Jöckel et al., 2006; Pozzer et al., 2007), and additional details about the model system can be found at <http://www.messy-interface.org>.

In this study, the applied spectral resolution of the ECHAM5 base model is T106, corresponding to a horizontal resolution of the quadratic Gaussian grid of $\approx 1.1^\circ \times 1.1^\circ$. The applied vertical resolution is 31 layers, up to 10 hPa. The model dynamics has been weakly nudged (Jeuken et al., 1996; Jöckel et al., 2006; Lelieveld et al., 2007) towards the analysis data of the European Centre for Medium-Range Weather Forecasts

**Aerosol simulation
with EMAC**

A. Pozzer et al.

[Title Page](#)[Abstract](#)[Introduction](#)[Conclusions](#)[References](#)[Tables](#)[Figures](#)[◀](#)[▶](#)[◀](#)[▶](#)[Back](#)[Close](#)[Full Screen / Esc](#)[Printer-friendly Version](#)[Interactive Discussion](#)

(ECMWF) operational model (up to 100 hPa) to represent the actual day-to-day meteorology in the troposphere. This allows a direct comparison with observations. The model output is 5-hourly, thus an entire daily cycle is covered after 5 days. Dry and wet deposition processes have been extensively described by Kerkweg et al. (2006a) (DRYDEP submodel) and Tost et al. (2006a, 2007a) (SCAV submodel), respectively, while the emission procedure has been explained by Kerkweg et al. (2006b) (OFFLEM, ONLEM and TNUDGE submodel) and Pozzer et al. (2006) (AIRSEA submodel). The chemistry is calculated with the MECCA submodel of Sander et al. (2005). The model setup does not include feedbacks between chemistry and dynamics. The other submodels used in this study are CONVECT (Tost et al., 2006b), LNOX (Tost et al., 2007b), as well as CLOUD, CVTRANS, JVAL, HETCHEM and TROPOP (Jöckel et al., 2006).

Aerosol microphysics and gas/aerosol partitioning are calculated by the Global Modal-aerosol eXtension (GMXe) aerosol module (described by Pringle et al., 2010b,a). GMXe simulates the distribution of sulfate, BC (Black Carbon), POM (Particulate Organic Matter), nitrate, ammonium, DU (Dust) and SS (Sea Spray) aerosol within 7 interacting lognormal modes (in a similar approach to that of Vignati et al., 2004; Stier et al., 2005; Mann et al., 2010). The particle number and mass of each mode is calculated prognostically but the geometric standard deviation is fixed (2.0 for the coarse modes hydrophobic, 2.2 for coarse mode hydrophilic, 1.59 for all other modes). The 7 lognormal modes span four size categories (nucleation (< 5 nm radius), Aitken (5–50 nm), accumulation (50–500 nm) and coarse (> 500 nm)) and are divided into a hydrophilic (4 modes) and a hydrophobic (3 modes) distribution. Hydrophobic aerosol (BC and DU) is emitted into the three modes in the hydrophobic distribution and hydrophilic aerosol (sulfate and sea spray) is emitted into the three largest modes of the 4-mode hydrophilic distribution. The emissions of POM are split between the hydrophobic (35 %) and hydrophilic (65 %) distributions. A parameterisation of aerosol ageing allows aerosol to pass from the hydrophobic to the hydrophilic distribution upon the addition of hydrophilic material (Vignati et al., 2004). The distribution of species with each mode is given in Pringle et al. (2010b, their Table 2). The aerosol within each

**Aerosol simulation
with EMAC**

A. Pozzer et al.

Title Page

Abstract

Introduction

Conclusions

References

Tables

Figures

◀

▶

◀

▶

Back

Close

Full Screen / Esc

Printer-friendly Version

Interactive Discussion



mode is internally mixed while the 7 modes are externally mixed with respect to each other. Gas/aerosol partitioning is treated using the ISORROPIA-II model (Fountoukis and Nenes, 2007; Nenes et al., 1998a,b). In this study ISORROPIA-II is used to treat the interaction of NH_4 , Na, SO_4 , NO_3 , Cl, H_2O aerosols. Gas-phase species considered are NH_3 , HCl, HNO_3 , H_2O . ISORROPIA-II solves for the equilibrium state by considering the chemical potential of the species (Nenes et al., 1998a,b). By considering specific compositional “regimes”, it minimises the number of equations and iterations required. In this study activity coefficients are taken from pre-calculated lookup tables to reduce computational expense (see also Pringle et al., 2010b).

The optical properties of the aerosol are calculated with the EMAC submodel AEROPT. It is based on the scheme by Lauer et al. (2007) and makes use of pre-defined lognormal modes (i.e. the mode width σ and the mode mean radius have to be taken into account), for which lookup tables with the extinction coefficient σ_{SW} , the single scattering albedo ω_{SW} and the asymmetry factor γ_{SW} for the shortwave and extinction coefficient σ_{LW} for the longwave spectrum have to be created.

These lookup tables are calculated with the help of the LIBRADTRAN (Mayer and Kylling, 2005) for various aerosol types. In the case of the AEROPT submodel the considered species are POM, BC, DU, SS, water soluble compounds (WASO, i.e. all other water soluble inorganic ions, e.g.: NH_4^+ , SO_4^{2-} , HSO_4^- , NO_3^- , etc.) and aerosol water (H_2O). The refractive indices for these compounds are taken from several data bases, e.g. HITRAN2004. The references used are:

- WASO (mainly using ammonium sulfate values following Hess et al., 1998),
- BC (Hess et al., 1998),
- SS (Shettle, 1979),
- H_2O (Hale and Query, 1973),
- OC (Hess et al., 1998; Sutherland and Khanna, 1991; S. Kinne, personal communication, 2010),

– DU (Hess et al., 1998; S. Kinne, personal communication, 2010).

For these compounds the wavelength dependent complex refractive index is used for a comprehensive set of Mie calculations. This results in a 3-dimensional lookup table (depending on the complex refractive index and the Mie size parameter, combining the wavelength and aerosol size information) spanning up a $100 \times 100 \times 100$ space.

During the simulation, the volume-weighted mean complex refractive index is determined for each mode of the aerosol distribution. Then, depending on the mean radius of the mode, the the Mie size parameter is calculated for each wavelength band. These three parameters provide the required information for the lookup table for the values for σ_{sw} , ω_{sw} , γ_{sw} and σ_{lw} . To cover the wavelength dependency these coefficients are determined for 16 predefined bands in the shortwave and 16 in the longwave spectrum, which are not necessarily required to match the bands used in the radiation calculation of the base model (in our case ECHAM5). Next a mapping of the precalculated wavelength bands to those of the radiation scheme is performed using a weighted interpolation. This method is also applied used to determine the values for other (diagnostic) wavelengths, e.g. for the 550 nm band, which is often used in observational data sets. The actual values for optical parameters (e.g. the AOD) are finally obtained by weighting the coefficients with the number of aerosol particles per grid cell.

The model simulation covers the years 2004–2008. The first year is used as spin-up for the model and only the years 2005–2008 are used in this study. These years are expected to be represented by the model with high consistency, because the chosen emission setup of primarily emitted species was compiled for the year 2005 (see below).

2.1.1 Emissions

The high resolution global anthropogenic emission inventory (1990–2005) which was used in this study has been prepared in the framework of the CIRCE Project (No. 036961) by the EDGAR group (EDGAR, Emission Database for Global

Aerosol simulation with EMAC

A. Pozzer et al.

Title Page

Abstract

Introduction

Conclusions

References

Tables

Figures

◀

▶

◀

▶

Back

Close

Full Screen / Esc

Printer-friendly Version

Interactive Discussion



Atmospheric Research) of the EC-Joint Research Center Ispra (Italy), Climate Change Unit (Doering et al., 2009a,c). This dataset includes greenhouse gases, NO_x, CO, NMVOCs, NH₃ and SO₂ from fossil fuel and biofuel related emissions. Emissions from international aviation were calculated for the period 1990–2005 using a technology based emission factor approach (Eyers et al., 2004). International shipping emissions are based on the QUANTIFY project (Hoor et al., 2009). The EDGAR-CIRCE emission database has been evaluated by Doering et al. (2009b), who compared this dataset to other emissions inventories; the EDGAR-CIRCE emissions are in line with other global (Bond et al., 2007; UNF, 2008) and regional (Ohara et al., 2007; Streets et al., 2003; Klimont et al., 2002; Vestreng and Klein, 2002) and the differences lie well within the uncertainties associated with emissions estimates. The anthropogenic emissions were distributed vertically as described in Pozzer et al. (2009), and the chosen vertical distribution of the emissions is based on the EMEP (European Monitoring and Evaluation Programme) model (Dimitroulopoulou and ApSimon, 1999; Simpson et al., 2003), applied after the analysis of stack plume data from Eastern Europe. As shown in Pozzer et al. (2009) and De Meij et al. (2006), correct injection height of the emissions is very important in global and regional models, leading to an improvement of up to 30 % in the correlation with station observations compared to simulations where the emissions are not vertically distributed. The CIRCE emissions dataset has a spatial resolution of 0.1 × 0.1°. The standard temporal resolution is annual, and only the data for year 2005 has been produced with higher resolution (monthly). Hence, in this study, only the emissions for the year 2005 have been used to take advantage of high temporal and spatial resolution. The biogenic emissions of organic species have been represented following Guenther et al. (1995) and are computed offline in the model (Ganzeveld et al., 2006) with monthly temporal resolution. The natural emissions of NH₃ are based on the GEIA database (Bouwman et al., 1997). Both these datasets have a 1 × 1° horizontal resolution. NO_x produced by lightning is calculated online and distributed on different vertical levels, based on the parametrization of Price and Rind (1992). The emission of NO from soils is calculated online based on the algorithm developed by

**Aerosol simulation
with EMAC**

A. Pozzer et al.

[Title Page](#)[Abstract](#)[Introduction](#)[Conclusions](#)[References](#)[Tables](#)[Figures](#)[◀](#)[▶](#)[◀](#)[▶](#)[Back](#)[Close](#)[Full Screen / Esc](#)[Printer-friendly Version](#)[Interactive Discussion](#)

Yienger and Levy (1995) and depends on ecosystem type, soil moisture state and the surface temperature. The underlying ecosystem map was compiled by Olson (1992) also used to estimate the isoprene emissions with the ONLEM submodel. Volcanic emissions of SO₂ are based on the AEROCOM data set (Dentener et al., 2006), with background emissions from continuous and explosive volcanoes. The biomass burning contribution was added using the Global Fire Emissions Database (GFED version 3, (van der Werf et al., 2010)) covering the years 1997–2009 with a 0.5° × 0.5° spatial resolution and a monthly temporal resolution. The AIRSEA submodel (Pozzer et al., 2006) calculates the oceanic DMS emissions online, with prescribed sea water DMS concentrations from Kettle et al. (1999). Additionally AIRSEA calculates isoprene emissions, where the water isoprene concentration was estimated from chlorophyll concentration (Conkright et al., 2002) based on the work of Broadgate et al. (2000). Finally, AIRSEA estimates the methanol (CH₃OH) water deposition, based on an undersaturation of the oceanic surface water of 0.94. The atmosphere-ocean transfer velocity parametrization is based on Wanninkhof (1992).

The total gas-phase emissions are shown in Table 1.

Anthropogenic bulk aerosol emissions are also based on the CIRCE EDGAR emissions inventory. Biomass burning BC and POM are based on the GFEDv3.1 emission database. Secondary Organic Aerosol (SOA) particles are directly emitted as POM, assuming that 15 % of natural terpene emissions form SOA (Guenther et al., 1995). Emission of dust and sea spray aerosol are treated using offline monthly emission files based on AEROCOM. Offline emission of dust and sea spray have been used in this study because of their extensive use and evaluation in a number of studies, and to increase the comparability with the work of Pringle et al. (2010a).

**Aerosol simulation
with EMAC**

A. Pozzer et al.

[Title Page](#)[Abstract](#)[Introduction](#)[Conclusions](#)[References](#)[Tables](#)[Figures](#)[◀](#)[▶](#)[◀](#)[▶](#)[Back](#)[Close](#)[Full Screen / Esc](#)[Printer-friendly Version](#)[Interactive Discussion](#)

2.2 Satellite observations

2.2.1 MISR

The Multi-angle Imaging SpectroRadiometer (Diner et al., 1998, MISR) instrument flies on the Terra satellite and has been operational since February 2000. The instrument is designed to measure the solar radiation reflected by the Earth system by a multiple camera configuration (four forward, one nadir and four backward). Each camera measures in four different wavelengths centred at 446 nm (blue), 558 nm (green), 671 nm (red) and 866 nm (near-infrared). In this study Level 3 Component Global Aerosol Product version F15 (CGAS-F15) are used, specifically the AOD (Average Optical Depth), which is derived from Level 1 and Level 2 products, averaged over a month and stored on a geographic grid of $0.5 \times 0.5^\circ$. A comparison over land and ocean with AERONET (AERosol RObotic NETwork) data has shown that MISR AODs are within 0.05–20% of that of AERONET (Kahn et al., 2005, 2010). MISR AODs can be obtained from <https://wist.echo.nasa.gov/api/>.

2.2.2 MODIS

The MODerate resolution Imaging Spectro-radiometer (MODIS) instrument also flies on the Terra satellite. In contrast to MISR, the MODIS instrument has only one camera which measures radiances in 36 spectral bands. Daily Level 2 (MOD04) aerosol optical depth products (550 nm) are produced on a spatial resolution of 10×10 km over land, using the $1 \text{ km} \times 1 \text{ km}$ cloud-free pixel size. The MODIS Level 2 product refers to a swath width of about 2330 km, therefore the instrument has almost daily global coverage. In this study global Level 3 AOD (version MOD08) Collection 005 products are used (field `Optical_Depth_Land_And_Ocean_Mean`). The level 3 AOD product is derived from the statistics of the Level 2 products and stored on a $1 \times 1^\circ$ grid in the MOD08 Level 3 product file. Reported MODIS AOD uncertainties are $\pm 0.05 \pm 0.15 \times \text{AOD}$ (Remer et al., 2008; Levy et al., 2010). Although MODIS

Aerosol simulation with EMAC

A. Pozzer et al.

Title Page

Abstract

Introduction

Conclusions

References

Tables

Figures

◀

▶

◀

▶

Back

Close

Full Screen / Esc

Printer-friendly Version

Interactive Discussion



aerosol products are provided over land (Kaufman et al., 1997) and water surfaces (Tanré et al., 1997), it is important to underline that no aerosol retrieval is possible over bright surfaces such as deserts and ice. MODIS AODs can be obtained from <https://wist.echo.nasa.gov/api/>.

2.3 In situ observations

2.3.1 CASTNET

The Clean Air Status and Trends Network (CASTNet) comprises 86 sites located in or near rural areas of the United States, administered and operated by the Clean Air Markets Division (CAMD) of the United States Environmental Protection Agency (EPA) (Edgerton et al., 1990). CASTNET is the USA's primary monitoring network for measuring concentrations of air pollutants. All sites utilize a Teflon filter to collect particulate sulfate (SO_4^{2-}), nitrate (NO_3^-), and ammonium (NH_4^+). The sampling is conducted on a weekly basis. The usage of Teflon filters in the network for nitrate particle collection is known to underestimate the effective concentration of NO_3^- (Ames and Malm, 2001), due to temperature-dependent volatilization (Hering and Cass, 1999), or by reaction with strong acids under ammonia limited conditions (Appel et al., 1988). In this work we only use data from stations with continuous coverage for the years 2005–2008 (33 stations in total).

2.3.2 EMEP

The European Monitoring and Evaluation Programme (EMEP) is a scientifically based and policy driven programme under the Convention on Long-range Transboundary Air Pollution for international co-operation to help solve transboundary air pollution problems. Parties to the Convention on Long-Range Transboundary Air Pollution perform monitoring at regional monitoring sites across Europe. The data are subject to national quality assessment prior to submission to the EMEP Chemical Coordinating Centre at

Aerosol simulation with EMAC

A. Pozzer et al.

Title Page

Abstract

Introduction

Conclusions

References

Tables

Figures

◀

▶

◀

▶

Back

Close

Full Screen / Esc

Printer-friendly Version

Interactive Discussion



NILU (Norwegian Institute for Air Research). The number of stations used in the comparison ranges from 59 (for SO_4^{2-}) to 31 (for NO_3^- and NH_4^+). Due to the partial usage of Teflon filters (depending on the station/country), observations from this network are also expected to underestimate NO_3^- concentrations.

2.3.3 EANET

The Acid Deposition Monitoring Network in East Asia (EANET) was established as an initiative for regional cooperation among the participating countries, creation of a common understanding of the state of acid deposition problems and for providing useful inputs to policy makers at various levels. Regular monitoring activities started in January 2001 with the participation of 10 countries, namely China, Indonesia, Japan, Malaysia, Mongolia, Philippines, Republic of Korea, Russia, Thailand, and Viet Nam. Cambodia, with Lao People's Democratic Republic and Myanmar joining EANET in 2001, 2002 and 2005, respectively. Acid deposition monitoring of EANET covers four environmental items: wet deposition, dry deposition (air concentration), soil and vegetation, and inland aquatic environment. In this work, data from 28 stations of the EANET network were used.

3 Comparison with observations

In the following sections, a comparison of the model results with observations is performed. All the observational data have been collected at (or reduced to) monthly averages. Firstly, the global AOD will be analysed, to give an overall picture of the model performance on a large scale. This comparison is important for regions where no direct information of concentrations are available. The explicit AOD calculation during the simulation allows a more detailed analysis than that performed by Pringle et al. (2010a), who in addition to using annual mean anthropogenic emission fields, used only an offline simplified treatment of AOD based on the parametrization of Kiehl and Briegleb (1993).

Aerosol simulation with EMAC

A. Pozzer et al.

Title Page

Abstract

Introduction

Conclusions

References

Tables

Figures

◀

▶

◀

▶

Back

Close

Full Screen / Esc

Printer-friendly Version

Interactive Discussion



After the evaluation of AOD, the simulated aerosol mass concentrations are compared to measurements taken from observational networks in North America, Europe and Asia.

3.1 Comparison with satellite observations

The differences of the 2005–2008 average AOD between the model and the satellite observations are shown in Fig. 1. In general, the AOD simulated by the model corresponds very well with the observations for large areas of the globe (with a difference below 0.07), particularly over remote marine regions. Good agreement is also found over Europe and Northeastern America.

A strong underestimation of the model with respect to the observed AODs (both for MODIS and MISR observations) is found in the tropical regions, especially over the Central Atlantic ocean, the Northern Indian Ocean, the Malaysian region and over the Gulf of Mexico. The underestimation could be related to the uncertainties (underestimation) in the emissions for dust and biomass burning in the inventory or a too fast deposition over marine regions. However, some underestimation of the emissions is most probable. Dust, in fact, is only emitted at the lowest level of the model, hence neglecting the strong dust plume episodes which can uplift and transport dust on a wider range. This is confirmed by a good spatial correlation of AOD between satellite and model results during winter season, when the dust storm episodes are reduced in number with respect to the summer season (see below). Additionally, the biomass burning emissions of BC and POM in the inventory (2.12 Tg yr^{-1} and 18.45 Tg yr^{-1} for BC and POM, respectively) may be underestimated, being lower than what suggested in the literature (3.1 and 34.7 Tg yr^{-1} , respectively, Dentener et al., 2006). The underestimations of the biomass burning sources has been noticed for the same simulation also for other emitted compounds (CO, Liu et al., 2011) when compared to satellite observations. The underestimation could possibly produce a bias in the AOD estimates by the model, which results in too low AODs when compared with MODIS and MISR, as observed e.g. over the Central Atlantic Ocean. The underestimation of AOD over the Northern Indian Ocean is consistent with an underestimation of the dust outflow from

Aerosol simulation with EMAC

A. Pozzer et al.

Title Page

Abstract

Introduction

Conclusions

References

Tables

Figures

◀

▶

◀

▶

Back

Close

Full Screen / Esc

Printer-friendly Version

Interactive Discussion



the Arabian peninsula, while the underestimation of the AODs over the Indian sub-continent indicates too low emissions of anthropogenic/biomass burning origin. The largest effect of the underestimation of the biomass burning emissions can be found over the Malaysian region, where the simulated AODs is consistently underestimated (~0.2) with respect to the MODIS and MISR observations. Over China (more specifically inland) the model tends to overestimate the AODs. The cause is not clear, as the next sections indicate that the model does not overestimate anthropogenic aerosol compounds in this region.

Further, the model shows discrepancies with the MODIS observations also over the western part of the USA and Canada. Generally, the model tends to agree more closely to MISR than MODIS observations. The MISR instrument registers AODs over bright surfaces, which allows us to evaluate calculated AODs e.g. over the Arabian peninsula. Over this region the model underestimates the observed AODs, most probably due to an underestimation of the dust emissions. Note that a new dust emission routine is under development for the EMAC model, to improve this aspect in the near future.

To further quantify the capability of the model to reproduce the spatial distribution of the AODs observed by MODIS and MISR, we present Taylor diagrams in Fig. 2 of the comparison on a monthly basis. It shows the correlation coefficient between model results and observations (R) by the angle to the ordinate. The standard deviation of the model normalised to the standard deviation of the observations ($\sigma_{\text{model}}/\sigma_{\text{obs}}$) is represented by the distance from the origin. The observations are therefore located at a correlation of 1 and a normalised standard deviation of 1. The distance between a point and this “ideal” point is the centered pattern root mean square. The better a model reproduces the observations, the closer the resulting points are located to this “ideal” point. A detailed explanation of this type of diagram has been presented by Taylor (2001). While the spatial correlation between model and observations is generally very good (higher than 0.5), the normalised standard deviation is below one, indicating that the strong spatial gradients between high AODs and low AODs are not well reproduced.

**Aerosol simulation
with EMAC**

A. Pozzer et al.

Title Page

Abstract

Introduction

Conclusions

References

Tables

Figures

◀

▶

◀

▶

Back

Close

Full Screen / Esc

Printer-friendly Version

Interactive Discussion



**Aerosol simulation
with EMAC**

A. Pozzer et al.

[Title Page](#)[Abstract](#)[Introduction](#)[Conclusions](#)[References](#)[Tables](#)[Figures](#)[◀](#)[▶](#)[◀](#)[▶](#)[Back](#)[Close](#)[Full Screen / Esc](#)[Printer-friendly Version](#)[Interactive Discussion](#)

The model reproduces the satellite observations with a high degree of consistency during winter time. As shown in Fig. 2, despite the relatively high correlation (0.6–0.7), for spring and summer months (April until September) we obtain a normalised standard deviation of the model compared to the observations of ~ 0.6 (MODIS) and ~ 0.4 (MISR). In autumn and winter the model simulates the AOD with a higher level of agreement. Not only the spatial correlation coefficients are around 0.5–0.6, but the normalised standard deviation is close to unity especially during January–March.

After the analysis of the spatial distribution for different months, the capability of the model to reproduce the seasonal cycle of the observed AODs is also investigated. The temporal correlation coefficients between the observations and model results are shown in Fig. 3. It indicates whether the model is able to reproduce the observed seasonal cycle (if any is present), independent of biases between observations and model results. A low correlation (close to zero) implies either a wrong representation of the seasonal cycle by the model or the lack of a well defined seasonal cycle in the model and/or observations. The temporal correlation is, w.r.t the MODIS and MISR observations, low over some oceanic regions (i.e. Southern Indian Ocean and Southern Pacific Ocean) due to the low seasonal variation in the emissions of sea salt. Outside Europe and the USA the information about the seasonal variation is often not available, which is one of the reasons that these variations are normally not included in global emission inventories of anthropogenic emissions (De Meij et al., 2006). Although the modelled AODs are generally lower than the observed AODs over Central Africa, the seasonality of the AOD reproduces the observations, with temporal correlation coefficients higher than 0.7. High temporal correlation coefficients (0.8) are also found over Malaysia, which indicates that the model is correct in timing the biomass burning emissions for this region. Very good correlation (higher than ~ 0.7) with both observational datasets is found for the Arabian region. This indicates that the timing of dust events in the regions (i.e. the transport) is correctly reproduced, at least partially related to the nudging technique. Nevertheless, as mentioned earlier, the calculated AODs are lower compared to the observed AODs, due to the constant emissions of dust in the model,

which are prescribed offline. A good correlation (~ 0.6 – 0.8) is obtained over the North Africa, the Central Atlantic Ocean and the Southern Europe when compared to MISR observations. This indicates that the dust intrusions over these regions are correctly timed by the model, although (as noticed before) their intensity is generally underestimated. It must however be underlined, that the modelled AOD in the dust outflow regions is strongly affected by the conversion rate from hydrophilic to hydrophobic via condensation and coagulation with hydrophilic material, and that it cannot be ruled out that this effect plays also a role in the AOD underestimation in these regions.

3.2 Station observations

To evaluate the calculated global concentrations of sulfate, nitrate and ammonium aerosols, the multiyear model results (2005–2008) are compared with measurements from different monitoring networks. We selected the stations for which data is available for the complete time period (i.e. between 2005–2008). In the scatter plots all the available data are shown (monthly values), while in the Taylor diagrams, the data are grouped per month, and all data available for a certain month (independent of the year) are used in the calculation. The Taylor diagrams, therefore, give information on the spatial correlations (and normalised standard deviation) between observations and model results for each month.

In Table 3, an overview of the comparison between the model results and the observations is presented, discussed in the following sections.

3.2.1 SO_4^{2-}

Overall the model correctly reproduces the observed concentrations of SO_4^{2-} , with more than 88 %, 92 % and 95 % of the model results within a factor of two of the observations based on the EANET, EMEP and CASTNET networks, respectively (see Table 3). The yearly average concentrations are reasonably well captured (see Fig. 4), indicating that the spatial gradients of the monthly mean concentrations are relatively well reproduced by the model. The model calculates high sulfate concentrations over

Aerosol simulation with EMAC

A. Pozzer et al.

[Title Page](#)[Abstract](#)[Introduction](#)[Conclusions](#)[References](#)[Tables](#)[Figures](#)[I◀](#)[▶I](#)[◀](#)[▶](#)[Back](#)[Close](#)[Full Screen / Esc](#)[Printer-friendly Version](#)[Interactive Discussion](#)

Europe and East USA (up to $9 \mu\text{g m}^{-3}$ and $7 \mu\text{g m}^{-3}$, respectively) and very high concentrations over East China and other parts of East Asia (up to $25 \mu\text{g m}^{-3}$). The East-West gradient in the USA and the South-North gradient in Europe are reproduced, while the gradients over East Asia are underestimated.

Figure 5 shows the comparison between the simulated SO_4^{2-} and the different observations network. The general underestimation of SO_4^{2-} by the model (see MAM/OAM in Table 3) is clear from the comparison with the CASTNET and EANET datasets (see Fig. 5, scatter plot) and partially in the comparison with the EMEP dataset. The general underestimation is also noticeable in the Taylor diagrams, where the normalised standard deviation is generally ~ 0.5 for comparison with CASTNET and EANET, while with EMEP it is between ~ 0.5 and ~ 1 . Notably, the lowest values of normalised standard deviations appear during winter months (November–January). During the summer months (June and July) the normalised standard deviations are close to the ideal value of 1. Again, the spatial correlation coefficient is generally above ~ 0.6 during most of the year, which implies a good representation of the spatial distribution of SO_4^{2-} throughout the year. The simulation results agree very well with the CASTNET network observations, where a spatial correlation higher than ~ 0.7 is achieved, with peaks of 0.95 during the Summer and Autumn. The comparison with the EMEP network observations again shows the lowest value of the spatial correlation during the winter season.

The general underestimation present in the model results compared to the CASTNET observations does not seem to influence the overall agreement of the seasonal cycle of SO_4^{2-} , which is very well reproduced in the USA (see Fig. 4, lower panel). In the USA the model reproduces (with a temporal correlation value above 0.7 in most locations) the observed seasonality, with the unique exception of stations located in the Central USA. Compared to EMEP and EANET, however, the model results have a somewhat lower temporal correlation (~ 0.5 – 0.6), which is due to the absence of a clear seasonal cycle in the observations and being more pronounced in the model (not shown).

**Aerosol simulation
with EMAC**

A. Pozzer et al.

Title Page

Abstract

Introduction

Conclusions

References

Tables

Figures

◀

▶

◀

▶

Back

Close

Full Screen / Esc

Printer-friendly Version

Interactive Discussion



3.2.2 NO₃⁻

NO₃⁻ is not reproduced with the same consistency as SO₄²⁻. Although the model seems to predict the observed average nitrate concentration with a minor overestimation over Europe and West USA (see Fig. 6), it clearly overestimates the NO₃⁻ concentrations over East Asia. Nevertheless, the seasonal cycle is generally well reproduced by the model (see Fig. 6, lower panel) both in the USA (with a temporal correlation coefficient of ~ 0.8–0.9) and in Japan (with temporal correlation coefficient between ~ 0.6 and 0.8), while a somewhat lower temporal correlation is calculated for some locations in Europe and West USA. The calculated mean is at least ~ 60 % higher than the observed values (see Table 3 and Fig. 7), for all network observations. This difference is possibly due to measurement biases in the networks. As mentioned in Sect. 2.2, the nitrate concentrations measured with teflon filters can be low biased, especially in warm and dry conditions, as nitrate evaporates from the filters (Ames and Malm, 2001). As shown by Schaap (2003); Schaap et al. (2004); De Meij et al. (2006), NH₄⁺ and NO₃⁻ evaporate partially from the filters at temperatures between 15 °C and 20 °C while at higher temperatures they can evaporate completely. It is hence possible that observational biases are responsible for the limited agreement between model results and the observations. A further indication of the possible evaporation of nitrate from the sampling filters is presented in the Taylor diagrams in Fig. 7. In the comparison with EANET the spatial correlation for summer months is outside the plots, indicating a strong overestimation of the model with respect to the observations. For the colder winter period (hence with lower evaporation of nitrate from the filters), the model results agree much better with the observations. In the case of CASTNET observations the spatial correlation coefficient is higher than 0.7 for December–March. Similarly, the model reproduces the EANET observations during November and December with a spatial correlation higher than 0.5, but the spatial correlation coefficients obtained for the spring and the other winter months are between 0.2 and 0.4, but with a good normalised standard deviation (~ 0.5, ~ 0.8, ~ 0.9 and ~ 0.9 for January–April, respectively). In addition, there is

Aerosol simulation with EMAC

A. Pozzer et al.

Title Page

Abstract

Introduction

Conclusions

References

Tables

Figures

◀

▶

◀

▶

Back

Close

Full Screen / Esc

Printer-friendly Version

Interactive Discussion



a large scatter between EANET observations and simulation results (confirmed by low correlations), caused by an overestimation of nitrate concentrations at marine sites. In contrast to the EANET observations, the model results agree well with the observed nitrate from the EMEP network, with a spatial correlation of ~ 0.5 – 0.6 and a normalised standard deviation between 0.5 and 1.5.

3.2.3 NH_4^+

As shown in Fig. 8, the NH_4^+ distribution is highly concentrated over continental regions, especially over India and China (Clarisse et al., 2009) and over Central Europe. The spatial distribution of NH_4^+ agrees very well with the observation for all three observational networks. Excellent agreement is achieved between the model and observations of the CASTNET network, with spatial correlation coefficients higher than ~ 0.8 (see Fig. 9) and with 87 % of the modelled values within a factor of two of the observations (see Table 3). Also the spatial distribution over Europe is well reproduced, with spatial correlation coefficients higher than ~ 0.6 .

Although the spatial distribution is well reproduced, some discrepancies are found in the temporal variation of NH_4^+ (see Fig. 8, lower panel). In fact, the model results and the observations correlate very well over Europe and East Asia (with temporal correlations generally above 0.7 and 0.5, respectively), but the model does not present temporal correlations with observations over the East USA. For these locations, the model calculates a double peak in the NH_4^+ concentration during spring (March) and autumn (September). For example, for the station Edgar Evins (Tennessee, USA) a small peak during September $\sim 1.7 \mu\text{g m}^{-3}$ and a large peak of $\sim 2.5 \mu\text{g m}^{-3}$ during March (monthly average) is modelled. This biannual maximum is a direct result of the seasonal cycle of the NH_3 emissions in the region, which have a clear maximum in March and a secondary peak in September. This seasonality is not seen in the observations, which show a single yearly maximum for this location around September of $\sim 2.4 \mu\text{g m}^{-3}$ (monthly average). The emission database seems to reproduce the fertilizer applications (Goebes et al., 2003) over the USA, while the importance of livestock appears to

Aerosol simulation with EMAC

A. Pozzer et al.

[Title Page](#)[Abstract](#)[Introduction](#)[Conclusions](#)[References](#)[Tables](#)[Figures](#)[I◀](#)[▶I](#)[◀](#)[▶](#)[Back](#)[Close](#)[Full Screen / Esc](#)[Printer-friendly Version](#)[Interactive Discussion](#)

be strongly underestimated. Emissions from livestock cause a yearly maximum at the end of summer and they should account for $\sim 80\%$ of the NH_3 emissions in the region (Battye et al., 2003). The EDGAR-CIRCE emission dataset groups both emissions sources as “agricultural” (see Doering et al., 2009a, and references therein), making it impossible to confirm this hypothesis and to establish the real reason of the incorrect seasonality in the emissions. A revision of the emissions for this region is strongly recommended.

3.2.4 Sea spray and sodium

Sea spray aerosol (SS) consists mainly of chloride and sodium (Millero, 2003), which may both be used as proxies for seasalt aerosol. However, chloride can react with acid gases like nitric acid, causing chloride loss to the gas phase (in the form of HCl) (McInnes et al., 1994). On the other hand, sodium does not evaporate and has only minor non-marine sources (White, 2008), and can be used to calculate the total SS concentration from the observed sodium concentration. Following the studies of Manders et al. (2010) and Millero (2003), it is estimated that around one third of sea salt mass is sodium. In this work SS has been speciated in three different components: as bulk species (14%), as chloride (51.6%) and as sodium (33.7%) (see Sect. 2.1 and Pringle et al., 2010a). Hence sodium can be directly compared with observations, and the result reflects also the SS distributions.

As shown in Fig. 10, sodium is overestimated at almost all stations in the CASTNET, EMEP and EANET networks. The overestimation is more pronounced over Europe than over the USA and East Asia. Furthermore, the seasonality of the SS aerosol concentration (see Fig. 10, lower panel) is correctly reproduced over East USA, North Europe and at some locations over Japan, while a low temporal correlation coefficient (below 0.4) is calculated for all other stations (especially inland). Over water the total column of SS is correctly reproduced, as indicated by the correct calculation of the AOD over oceanic areas (see Sect. 3.1). It must be mentioned that in this study, the hydrophilic coarse mode is assumed to have a geometric standard deviation (σ) of 2.2,

Aerosol simulation with EMAC

A. Pozzer et al.

Title Page

Abstract

Introduction

Conclusions

References

Tables

Figures

◀

▶

◀

▶

Back

Close

Full Screen / Esc

Printer-friendly Version

Interactive Discussion



**Aerosol simulation
with EMAC**

A. Pozzer et al.

Title Page

Abstract

Introduction

Conclusions

References

Tables

Figures

I◀

▶I

◀

▶

Back

Close

Full Screen / Esc

Printer-friendly Version

Interactive Discussion



leading to a relative high dry deposition rate and sedimentation over land. This increase in the hydrophilic coarse mode geometric standard deviation was suggested by a previous horizontally coarser numerical experiment with a similar set up of the EMAC model (Pringle et al., 2010a), which showed an overestimation of a factor of two compared to observations, analogously to that obtained by Stier et al. (2005). This overestimation is not only still present in this study, but it even increased, with a general overestimation of a factor of ~ 3 (see Table 3). Hence, this study indicates that the SS overestimation is not only dependent on the horizontal resolution (as speculated by Pringle et al., 2010a; Stier et al., 2005). The coarse vertical resolution can be the cause of the SS overestimation over land, with the model unable to capture the correct deposition and sedimentation at the lowest level. As shown by Maring et al. (2003), SS is distributed vertically following a logarithmic profile, which is very difficult to reproduce with a coarse vertical resolution as in EMAC, with the first level being centered at ~ 30 m and with a vertical extension of ~ 60 m. An improved deposition function is needed in future simulations to describe the sea spray distribution more accurately.

4 Global and regional budgets

Owing to the relatively high resolution in space and time of the simulation performed in this study, global and local budgets for aerosol compounds (and precursors) can be estimated. In Table 4 the global budget for some species is presented. The bulk species (dust, seas salt, black carbon and particulate organic matter) follow similar results compared to previous work. The ratio of wet deposition to total deposition is in good agreement with what has been estimated by Textor et al. (2006), with 24 %, 30 %, 79 % and 80 % for dust, sea salt, BC and POM, respectively. Although the burdens of dust and sea salt are about half of that reported by Textor et al. (2006), these values are well within the standard deviation estimated from the multimodel ensemble in the same work.

**Aerosol simulation
with EMAC**

A. Pozzer et al.

[Title Page](#)[Abstract](#)[Introduction](#)[Conclusions](#)[References](#)[Tables](#)[Figures](#)[◀](#)[▶](#)[◀](#)[▶](#)[Back](#)[Close](#)[Full Screen / Esc](#)[Printer-friendly Version](#)[Interactive Discussion](#)

Emissions of SO_x , NH_3 and NO_y (with $108.1 \text{ Tg Syr}^{-1}$, 41.0 Tg Nyr^{-1} and $40.0 \text{ Tg N yr}^{-1}$) are similar to that estimated in the literature (see for example Pye et al., 2009; Bauer et al., 2007; Feng and Penner, 2007; Rodriguez and Dabdub, 2004). Wet deposition of SO_4^{2-} is similar to that obtained by Rodriguez and Dabdub (2004) and Pringle et al. (2010a), while it is around twice the estimate of Pye et al. (2009). Ammonium wet deposition ($21.0 \text{ Tg N yr}^{-1}$) is almost coincident with the results of Pye et al. (2009) and Feng and Penner (2007). Finally, wet deposition of nitrate ($18.9 \text{ Tg N yr}^{-1}$) is similar to that obtained by Rodriguez and Dabdub (2004), but around $\sim 25\%$ lower than that obtained by Pringle et al. (2010a) with the same model but different emissions. Also the dry deposition of these species are in line with the literature estimates.

Regional budgets were also calculated for five specific continents; Europe, North America, South America, Central Africa and Asia, presented in Table 5.

As expected the largest dust burdens are present over Europe, Central Africa and East Asia. While over Europe and Central Africa the dust is imported from outside the regions ($\sim 34 \text{ Tg yr}^{-1}$ each), in East Asia dust is locally emitted ($\sim 46 \text{ Tg yr}^{-1}$). Interestingly, dust is also differently deposited in these regions: while for Europe and Central Africa the wet deposition is the main sink, for East Asia sedimentation plays the main role. Near the source, in fact, the particles are relatively large and removed more efficiently by sedimentation. Sulfate aerosol has the largest burdens over industrialised regions (Europe, North America and East Asia), and it is at least a factor of 2 lower over Central Africa and South America. North America is a net exporter of all the compounds investigated, with the exception of SS. Analogously to North America, also Europe is a net exporter of most of species, with the exception of dust and sea salt. The European budget estimated in this work is in line with that obtained by Aan de Brugh et al. (2011). Europe is a net importer of dust and sea salt, with ~ 34 and $\sim 2 \text{ Tg yr}^{-1}$, respectively. The import of sea salt occurs from the Atlantic Ocean, related to the prevailing westerly winds. Compared to the regional anthropogenic emissions inventory EMEP (Vestreng et al., 2007, 2009), the emissions used in this work are significantly higher. As an example SO_2 emissions used here are $\sim 80\%$ higher

compared to the EMEP inventory (9.9 and 5.5 Tg S yr⁻¹, respectively), while smaller differences are present for NO_x (4.7 and 3.9 Tg N yr⁻¹, respectively) and NH₃ (5.3 and 3.5 Tg N yr⁻¹, respectively). Nevertheless the total SO_x, NO_y and NH₃ emissions in this work (11.2 Tg S yr⁻¹, 5.1 Tg N yr⁻¹ and 5.3 Tg N yr⁻¹, respectively) are in line with the work of Aan de Brugh et al. (2011) (11.4 Tg S yr⁻¹, 7.2 Tg N yr⁻¹ and 6 Tg N yr⁻¹, respectively), who used different anthropogenic emissions (Dentener et al., 2006). In contrast to other industrialised regions, East Asia is a net importer of NH₃. In general, NH₃ is transferred to the aerosol phase within the domain and washed out rapidly, as indicated by the relatively large amount of wet deposited NH₄⁺ (~3.5 Tg N yr⁻¹). East Asia is clearly a strong exporter of sulfate, with around ~34% of the global anthropogenic SO₂ emission (and ~25% of the total SO_x emission) being concentrated in the region. Although the SO_x emissions (~24 Tg S yr⁻¹) are more than twice the emissions in Europe (~11 Tg S yr⁻¹), most of the sulfur is converted to sulfate and washed out within the region, leading to an export (~2.2 Tg S yr⁻¹) that is comparable to that from Europe (~1.9 Tg S yr⁻¹). This has also been concluded by other studies (Lawrence et al., 2007). The EDGAR-CIRCE anthropogenic emissions in this region are quite different from those estimated by the REAS (Regional Emission inventory in ASia) database (Ohara et al., 2007) for the year 2005, although the differences are well within the errors associated with the emissions estimates of the region. The anthropogenic emissions used in this work are within 20% of the REAS database for BC (~1.4 and 1.3 Tg yr⁻¹, respectively) and NO_x (~6.8 and ~6.0 Tg N yr⁻¹, respectively), but quite different values are found for NH₃ (~6.1 and ~10.4 Tg N yr⁻¹, respectively), SO₂ (~24.0 and ~18.2 Tg S yr⁻¹, respectively) POM (~5.5 and ~3.9 Tg yr⁻¹, respectively). Nevertheless these values are in line with the literature estimates for these compounds (Streets et al., 2003; Streets and Waldhoff, 2000). This emphasizes the difficulties of constraining the emissions in this region. As expected, Central Africa and South America strongly export POM (~1.1 and 2.4 Tg (POM) yr⁻¹, respectively), due to the vegetation emissions and strong biomass burning events in these regions.

**Aerosol simulation
with EMAC**

A. Pozzer et al.

Title Page

Abstract

Introduction

Conclusions

References

Tables

Figures

◀

▶

◀

▶

Back

Close

Full Screen / Esc

Printer-friendly Version

Interactive Discussion



**Aerosol simulation
with EMAC**

A. Pozzer et al.

Title Page

Abstract

Introduction

Conclusions

References

Tables

Figures

◀

▶

◀

▶

Back

Close

Full Screen / Esc

Printer-friendly Version

Interactive Discussion



In Central Africa the intrusion of dust is comparable to Europe, with wet deposition playing a major role in the sink terms. Additionally, this relatively clean region is a net importer of most of the compounds with the exception of NO_y , which is emitted from biogenic activities and from biomass burning (~ 0.5 and 1.2 Tg N yr^{-1} , respectively).

5 South America (mainly the Amazon basin) is a largely pristine region with highly localised industrial sources. The sulfate aerosol, for example, is much lower compared to industrialised regions, though around a factor of 5 higher than that estimated for Central Africa. Overall, there is a net export of sulfate compounds. Similarly to Central Africa, the South American continent also exports nitrogen compounds ($\sim 0.8 \text{ Tg N yr}^{-1}$), due to the biogenic and biomass burning emissions.

5 Effect of monthly distribution of anthropogenic emissions

As mentioned in Sect. 2.1.1, the EDGAR-CIRCE inventory contains emissions on a relatively high spatial resolution with monthly temporal variation.

To evaluate the impact of the temporal distribution on the calculated aerosol concentrations, an additional model simulation (named NS, No Seasonality) was performed and the results were compared with the calculated concentrations of the standard simulation described in this work (here named ST, STandard case). Due to the intensive computational time requirement for these model simulations, simulation NS covers only the year 2005. The year 2005 is expected to be represented by the model with the highest consistency, mainly because the chosen emissions of primarily emitted species was compiled for this year. The model set-up of simulation NS is the same as in simulation ST, (described in Sect. 2.1), but without the monthly distribution of the anthropogenic components, i.e. neglecting the seasonal cycle present in the EDGAR-CIRCE database. Hence, the annual total emissions are not changed.

15 In Table 6 the results of NS and ST are compared with observations for different aerosol species for the year 2005. For SO_4^{2-} the calculated yearly averages by NS indicates a low bias relative to the observations compared to ST, while for all other species ST represents the yearly average better.

**Aerosol simulation
with EMAC**

A. Pozzer et al.

Title Page

Abstract

Introduction

Conclusions

References

Tables

Figures

◀

▶

◀

▶

Back

Close

Full Screen / Esc

Printer-friendly Version

Interactive Discussion



The comparison of SO_4^{2-} , NO_3^- , and Na^+ with the EANET network does not show significant differences between the two simulations. This is generally due to the small seasonal cycle present in the EDGAR-CIRCE data for East Asia. For example, SO_2 emissions in China do not show a strong seasonal cycle (Zhang et al., 2009), because of the continual energy production for industry and domestic usage. Therefore, neglecting the seasonal cycle hardly affects the calculated concentrations in this region. The comparison of model results from simulations NS and ST with CASTNET observation suggests large differences, especially for SO_4^{2-} . The bias is smaller for NS than ST when compared to the observations. This is caused by the strong monthly variability in the SO_2 emissions over the USA. The SO_2 emissions show a difference of a factor of 2 between winter and summer emissions (being lower in summer). Photochemical oxidation is a very important source of aerosol formation which contributes more than 50 % of the SO_4^{2-} formation, being larger in summer than winter. In NS, the SO_2 emissions are higher in the summer than in ST, which leads to higher SO_4^{2-} concentrations, also due to the relatively efficient photochemical oxidation of SO_2 . During winter, lower emissions of SO_2 in NS do not influence the calculated SO_4^{2-} concentrations, because of the reduced photochemical oxidation. Analogously, this effect is also observed for NO_3^- concentrations and the related NO_x emissions (although less strongly); also in this case, the yearly average is somewhat higher in simulation NS than in simulation ST, especially when compared to CASTNET. The temporal correlation of NS with the observations is somewhat lower than for ST, with a decrease of $\sim 10\%$ for SO_4^{2-} and 5% for NO_3^- , depending on the station.

In contrast to SO_4^{2-} and NO_3^- , the concentrations of NH_4^+ depend mainly on the sources of NH_3 , emitted by livestock and fertiliser usage, which are higher during the spring/summer months because of the intense agricultural activities during that period. Ignoring the temporal distribution of NH_3 emissions in NS shows a strong impact on the calculated NH_4^+ concentrations and confirms the findings by De Meij et al. (2006) and Schaap et al. (2004). Calculated NH_4^+ concentrations by ST show a smaller bias

than NS (see Table 6) and the model percentages of agreement within a factor of two to the observations, are higher for ST than NS with 3.6, 4.3 and 0.9 % increase when compared to CASTNET, EMEP and EANET, respectively. As shown in Fig. 12, the temporal correlation between model results and EMEP and EANET observations generally decreases ($\sim 10\%$) when the temporal distribution of the NH_3 emissions is ignored. It is interesting to see that NS correlates better with CASTNET than ST. As mentioned earlier, this may be related to the dual peak in the seasonal cycle of the NH_3 emissions not present in the observations (see Sect. 3.2.3). The lack of seasonality in NS improves the temporal correlation for many stations especially in the eastern part of the USA, although it remains rather low for many stations.

The spatial correlation coefficients between model results and observations show small differences for all aerosol species included in this study. The underlying reason for this is that the overall spatial distribution of the emissions does not change between the two simulations, rather showing the same patterns over the year. Finally, the impact of changing the monthly distribution on Na^+ concentrations is negligible. The reason for this is that the main emission source of Na^+ is mostly natural (i.e. sea spray) and therefore calculated concentrations do not change between the two simulations.

6 Conclusions

The newly produced global anthropogenic emission inventory (EDGAR-CIRCE) of pollutant gas and aerosol emissions has been incorporated in to the chemistry general circulation model EMAC (ECHAM5/MESSy Atmospheric Chemistry). The emission database not only provides a very high spatial resolution, but also a temporal distribution not present in other databases previously produced by the EDGAR community. The results covering the years 2005–2008 were compared with observations from satellites and regional networks to evaluate the model. The calculated AODs agree well with the satellite observations (level 3 products) over most of the globe, with a negative bias present in equatorial areas and in the dust outflow regions (i.e. Central Atlantic and Northern Indian Ocean). This is due to an underestimation of biomass burning

Aerosol simulation with EMAC

A. Pozzer et al.

[Title Page](#)[Abstract](#)[Introduction](#)[Conclusions](#)[References](#)[Tables](#)[Figures](#)[◀](#)[▶](#)[◀](#)[▶](#)[Back](#)[Close](#)[Full Screen / Esc](#)[Printer-friendly Version](#)[Interactive Discussion](#)

**Aerosol simulation
with EMAC**

A. Pozzer et al.

[Title Page](#)[Abstract](#)[Introduction](#)[Conclusions](#)[References](#)[Tables](#)[Figures](#)[◀](#)[▶](#)[◀](#)[▶](#)[Back](#)[Close](#)[Full Screen / Esc](#)[Printer-friendly Version](#)[Interactive Discussion](#)

and aeolian dust emissions. The AOD over industrialised regions is well reproduced although with some overestimation over East Asia and an underestimation near the west coast of the USA. Because the level 3 products do not present information about the sampling time, a more detailed study of the AOD produced by the model would be helpful, especially in comparison with level 2 products (i.e. with higher spatial and temporal resolution) to estimate the correct timing of pollution episodes and to quantify in more detail the simulation quality over industrialised regions.

Compared to regional network observations of aerosols, the model reproduces the main spatial and temporal atmospheric distribution of the sulfate, ammonium and nitrate aerosols. More specifically, good agreement is found for the simulated spatial distribution of sulfate and ammonium, while nitrate shows some differences when compared to observations. The temporal development of these aerosol species are in line with measurements, with the exception of ammonium aerosol, which shows some deviations from observations over the USA, mainly due to wrong emissions of ammonia from livestock. Finally, sodium, used as a proxy for the sea spray aerosol, shows an overestimation, previously seen with similar models, which may be related to a lack of detail in the representation of gradients in coastal regions, requiring improved emission and deposition parametrizations.

The usage of monthly varying anthropogenic emissions improves the model ability to reproduce the observations compared to yearly constant emissions, with an improved temporal correlation between 5 to 10 %, depending on the aerosol type and the location. The only exception appears for NH_4^+ , for which neglecting the seasonal cycle improved the simulation results over the USA, partially correcting the wrong seasonal distribution of the emissions. This improvement is, however, limited to the USA, while in the other regions a degradation of the model results compared to the observations is obtained.

In conclusion, the emission database EDGAR-CIRCE is found to be a valuable inventory for tropospheric chemistry and aerosol studies, with only a minor issue in the emission of ammonia in the Eastern USA, and its usage can be encouraged to

the atmospheric chemistry community, especially regarding its highly detailed spatial/temporal resolution.

Acknowledgements. We thank the DEISA Consortium (www.deisa.eu), co-funded through the EU FP6 project RI-031513 and the FP7 project RI-222919, for support within the DEISA Extreme Computing Initiative. The simulations for this study have been performed in the DEISA grid. We acknowledge support from the European Research Council (ERC) under the C8 project. We acknowledge the usage of data from the CIRCE project (contract number 036961). The authors wish also to acknowledge the use of the Ferret program for analysis and graphics in this paper. Ferret is a product of NOAA's Pacific Marine Environmental Laboratory (information is available at <http://www.ferret.noaa.gov>).

The service charges for this open access publication have been covered by the Max Planck Society.

References

- Aan de Brugh, J. M. J., Schaap, M., Vignati, E., Dentener, F., Kahnert, M., Sofiev, M., Huynen, V., and Krol, M. C.: The European aerosol budget in 2006, *Atmos. Chem. Phys.*, 11, 1117–1139, doi:10.5194/acp-11-1117-2011, 2011. 25227, 25228
- Adams, P. J. and Seinfeld, J. H.: Predicting global aerosol size distribution in general circulation models, *J. Geophys. Res.*, 107, 4370, doi:10.1029/2001JD001010, 2002. 25208
- Adams, P. J., Seinfeld, J. H., and Koch, D.: Global concentrations of tropospheric sulfate, nitrate, and ammonium aerosol simulated in a general circulation model, *J. Geophys. Res.*, 104, 13791–13824, doi:10.1029/1999JD900083, 1999. 25208
- Ames, R. and Malm, W.: Comparison of sulfate and nitrate particle mass concentrations measured by IMPROVE and the CDN, *Atmos. Environ.*, 35, 905–916, doi:10.1016/S1352-2310(00)00369-1, 2001. 25216, 25223
- Appel, B., Tokiwa, Y., Kothny, E., Wu, R., and Povard, V.: Evaluation of procedures for measuring atmospheric nitric acid and ammonia, *Atmos. Environ.*, 22, 1565–1573, 1988. 25216
- van Aardenne, J., Dentener, F., Olivier, J., Peters, J., and Ganzeveld, L.: The EDGAR 3.2 Fast Track 2000 Dataset (32FT2000), <http://www.mnp.nl/edgar/model/v32ft2000edgar/docv32ft2000/>, 2005. 25208

Aerosol simulation with EMAC

A. Pozzer et al.

Title Page

Abstract

Introduction

Conclusions

References

Tables

Figures

◀

▶

◀

▶

Back

Close

Full Screen / Esc

Printer-friendly Version

Interactive Discussion



**Aerosol simulation
with EMAC**

A. Pozzer et al.

Title Page

Abstract

Introduction

Conclusions

References

Tables

Figures

◀

▶

◀

▶

Back

Close

Full Screen / Esc

Printer-friendly Version

Interactive Discussion



Battye, W., Aneja, V. P., and Roelle, P. A.: Evaluation and improvement of ammonia emissions inventories, *Atmos. Environ.*, 37, 3873–3883, doi:10.1016/S1352-2310(03)00343-1, 2003. 25225

Bauer, S. E. and Koch, D.: Impact of heterogeneous sulfate formation at mineral dust surfaces on aerosol loads and radiative forcing in the Goddard Institute for Space Studies general circulation model, *J. Geophys. Res.*, 110, D17202, doi:10.1029/2005JD005870, 2005. 25208

Bauer, S. E., Koch, D., Unger, N., Metzger, S. M., Shindell, D. T., and Streets, D. G.: Nitrate aerosols today and in 2030: a global simulation including aerosols and tropospheric ozone, *Atmos. Chem. Phys.*, 7, 5043–5059, doi:10.5194/acp-7-5043-2007, 2007. 25227

Bond, T., Bhardwaj, E., Dong, R., Jogani, R., Jung, S., Roden, C., Streets, D., and Trautmann, N.: Historical emissions of black and organic carbon aerosol from energy-related combustion, 1850–2000, *Global Biogeochem. Cy.*, 21, GB2018, doi:10.1029/2006GB002840, 2007. 25213

Bouwman, A., Lee, D., Asman, W., Dentener, F., Van Der Hoek, K., and Olivier, J.: A global high-resolution emission inventory for ammonia, *Global Biogeochem. Cy.*, 4, 561–587, 1997. 25213

Broadgate, W., Liss, P., and Penkett, A.: Seasonal emission of isoprene and other reactive hydrocarbon gases from the ocean, *Geophys. Res. Lett.*, 24, 2675–2678, 2000. 25214

Clarisse, L., Clerbaux, C., Dentener, F., Hurtmans, D., and Coheur, P.-F.: Global ammonia distribution derived from infrared satellite observations, *Nat. Geosci.*, 2(7), 479–483, doi:10.1038/ngeo551, 2009. 25224

Conkright, M., O'Brien, T., Stephens, C., Locarnini, R., Garcia, H., Boyer, T., and Antonov, J.: *World Ocean Atlas 2001, Vol. 6: Chlorophyll*, NOAA Atlas NESDIS 52, US Government Printing Office, 46 pp., 2002. 25214

Dentener, F., Kinne, S., Bond, T., Boucher, O., Cofala, J., Generoso, S., Ginoux, P., Gong, S., Hoelzemann, J. J., Ito, A., Marelli, L., Penner, J. E., Putaud, J.-P., Textor, C., Schulz, M., van der Werf, G. R., and Wilson, J.: Emissions of primary aerosol and precursor gases in the years 2000 and 1750 prescribed data-sets for AeroCom, *Atmos. Chem. Phys.*, 6, 4321–4344, doi:10.5194/acp-6-4321-2006, 2006. 25214, 25218, 25228, 25245

Dimitroulopoulou, C. and ApSimon, H. M.: The influence of the photolysis rates on modelled ozone concentrations, *Atmos. Environ.*, 33, 147–154, 1999. 25213

Diner, D., Beckert, J., Reilly, T., Bruegge, C., Conel, J., Kahn, R., Martonchik, J., Ackerman, T., Davies, R., Gerstl, S., Gordon, H., Muller, J.-P., Myneni, R., Sellers, P., Pinty, B., and Ver-

Aerosol simulation with EMAC

A. Pozzer et al.

Title Page

Abstract

Introduction

Conclusions

References

Tables

Figures

◀

▶

◀

▶

Back

Close

Full Screen / Esc

Printer-friendly Version

Interactive Discussion



straete, M.: Multi-angle Imaging SpectroRadiometer (MISR) instrument description and experiment overview, *IEEE T. Geosci. Remote*, 36, 3113–3136, doi:10.1109/36.700992, 1998. 25215

Doering, U., Monni, S., Pagliari, V., Orlandini, L., van Aardenne, and SanMartin, F.: CIRCE report D8.1.1 – Emission inventory for the past period 1990–2005 on 0.1×0.1 grid, Tech. rep., Project FP6: 6.3, No. 036961, 2009a. 25213, 25225

Doering, U., van Aardenne, J., Monni, S., Pagliari, V., Orlandini, L., and SanMartin, F.: CIRCE report D8.1.2 – Evaluation emission database 1990–2005, Tech. rep., Project FP6: 6.3, No. 036961, 2009b. 25213

Doering, U., van Aardenne, J., Monni, S., Pagliari, V., Orlandini, L., and SanMartin, F.: CIRCE report D8.1.3 – Update of gridded emission inventories, addition of period 1990–2005 and the years 2010, 2015, 2050, Tech. rep., Project FP6: 6.3, No. 036961, 2009c. 25213

Edgerton, E., Lavery, T., Hodges, M., and Bowser, J.: National Dry Deposition Network: Second Annual Progress Report (1988), Epa/600/3-90/020, Environmental Protection Agency, Research Triangle Park, NC, 1990. 25216

Eyers, C. J., Addleton, D., Atkinson, K., Broomhead, M. J., Christou, R., Elliff, T., Falk, R., Gee, I., Lee, D., Marizy, C., Michot, S., Middel, J., Newton, P., Norman, P., Plohr, M., Raper, D., and Stanciou, N.: AERO2k, Global Aviation Emissions Inventories for 2002 and 2025, Tech. rep., QinetiQ Ltd, Farnborough, Hampshire QINETIQ/04/01113, 2004. 25213

Feng, Y. and Penner, J.: Global modeling of nitrate and ammonium: interaction of aerosols and tropospheric chemistry, *J. Geophys. Res.*, 112, D01304, doi:10.1029/2005JD006404, 2007. 25208, 25227

Fountoukis, C. and Nenes, A.: ISORROPIA II: a computationally efficient thermodynamic equilibrium model for $K^+ - Ca^{2+} - Mg^{2+} - NH_4^+ - Na^+ - SO_4^{2-} - NO_3^- - Cl^- - H_2O$ aerosols, *Atmos. Chem. Phys.*, 7, 4639–4659, doi:10.5194/acp-7-4639-2007, 2007. 25211

Ganzeveld, L. N., van Aardenne, J. A., Butler, T. M., Lawrence, M. G., Metzger, S. M., Stier, P., Zimmermann, P., and Lelieveld, J.: Technical Note: Anthropogenic and natural offline emissions and the online EMISSIONS and dry DEPOSITION submodel EMDEP of the Modular Earth Submodel system (MESSy), *Atmos. Chem. Phys. Discuss.*, 6, 5457–5483, doi:10.5194/acpd-6-5457-2006, 2006. 25213

Goebes, M. D., Strader, R., and Davidson, C.: An ammonia emission inventory for fertilizer application in the United States, *Atmos. Environ.*, 37, 2539–2550, doi:10.1016/S1352-2310(03)00129-8, <http://www.sciencedirect.com/science/article/B6VH3-48FSTR8-1/2/>

**Aerosol simulation
with EMAC**

A. Pozzer et al.

Title Page

Abstract

Introduction

Conclusions

References

Tables

Figures

◀

▶

◀

▶

Back

Close

Full Screen / Esc

Printer-friendly Version

Interactive Discussion



5b50e00b1973d85b2d72c54228158423, 2003. 25224

Guenther, A., Hewitt, C. N., Erickson, D., Fall, R., Geron, C., Graedel, T., Harley, P., Klinger, L.,
Lerdau, M., McKay, W. A., Pierce, T., Scholes, B., Steinbrecher, R., Tallamraju, R., Taylor, J.,
and Zimmerman, P.: A global model of natural volatile organic compound emissions, *J. Geo-*
phys. Res., 100, 8873–8892, 1995. 25213, 25214

Hale, G. and Querry, M.: Optical constants of water in the 200-nm to 200- μm wavelength region,
Appl. Optics, 12, 555–563, 1973. 25211

Hering, S. and Cass, G.: The magnitude of bias in the measurement of $\text{PM}_{2.5}$ arising from
volatilization of particulate nitrate from Teflon filters, *J. Air Waste Manage.*, 46(6), 725–733,
1999. 25216

Hess, M., Koepke, P., and Schult, I.: Optical properties of aerosols and clouds: the software
package OPAC, *B. Am. Meteorol. Soc.*, 79, 831–844, 1998. 25211, 25212

Hoor, P., Borcken-Kleefeld, J., Caro, D., Dessens, O., Endresen, O., Gauss, M., Grewe, V.,
Hauglustaine, D., Isaksen, I. S. A., Jöckel, P., Lelieveld, J., Myhre, G., Meijer, E., Olivier, D.,
Prather, M., Schnadt Poberaj, C., Shine, K. P., Staehelin, J., Tang, Q., van Aardenne, J.,
van Velthoven, P., and Sausen, R.: The impact of traffic emissions on atmospheric ozone
and OH: results from QUANTIFY, *Atmos. Chem. Phys.*, 9, 3113–3136, doi:10.5194/acp-9-
3113-2009, 2009. 25213

Huntingford, C., Hemming, D., Gash, J., Gedney, N., and Nuttall, P.: Impact of climate change
on health: what is required of climate modellers?, *T. Roy. Soc. Trop. Med. H.*, 101, 97–103,
doi:10.1016/j.trstmh.2006.11.001, 2007. 25207

Isaksen, I., Granier, C., Myhre, G., Berntsen, T., Dalsøren, S., Gauss, M., Klimont, Z., Benes-
tad, R., Bousquet, P., Collins, W., Cox, T., Eyring, V., Fowler, D., Fuzzi, S., Jöckel, P., Laj, P.,
Lohmann, U., Maione, M., Monks, P., Prevot, A. S. H., Raes, F., Richter, A., Rognerud, B.,
Schulz, M., Shindell, D., Stevenson, D. S., Storelvmo, T., Wang, W.-C., van Weele, M., Wild,
M., and Wuebbles, D.: Atmospheric composition change: climate-chemistry interactions,
Atmos. Environ., 43, 5138–5192, 2009. 25207

Jeuken, A., Siegmund, P., Heijboer, L., Feichter, J., and Bengtsson, L.: On the potential as-
similating meteorological analyses in a global model for the purpose of model validation,
J. Geophys. Res., 101, 16939–16950, 1996. 25209

Jöckel, P., Sander, R., Kerkweg, A., Tost, H., and Lelieveld, J.: Technical Note: The Modu-
lar Earth Submodel System (MESSy) – a new approach towards Earth System Modeling,
Atmos. Chem. Phys., 5, 433–444, doi:10.5194/acp-5-433-2005, 2005. 25209

Aerosol simulation with EMAC

A. Pozzer et al.

Title Page

Abstract

Introduction

Conclusions

References

Tables

Figures

◀

▶

◀

▶

Back

Close

Full Screen / Esc

Printer-friendly Version

Interactive Discussion



- Jöckel, P., Tost, H., Pozzer, A., Brühl, C., Buchholz, J., Ganzeveld, L., Hoor, P., Kerkweg, A., Lawrence, M. G., Sander, R., Steil, B., Stillier, G., Tanarhte, M., Taraborrelli, D., van Aardenne, J., and Lelieveld, J.: The atmospheric chemistry general circulation model ECHAM5/MESSy1: consistent simulation of ozone from the surface to the mesosphere, *Atmos. Chem. Phys.*, 6, 5067–5104, doi:10.5194/acp-6-5067-2006, 2006. 25209, 25210
- 5 Kahn, R. A., Gaitley, B. J., Martonchik, J. V., Diner, D. J., Crean, K. A., and Holben, B.: Multiangle Imaging Spectroradiometer (MISR) global aerosol optical depth validation based on 2 years of coincident Aerosol Robotic Network (AERONET) observations, *J. Geophys. Res.*, 110, 0148–0227, doi:10.1029/2004JD004706, 2005. 25215
- 10 Kahn, R. A., Gaitley, B. J., Garay, M., Diner, D. J., Eck, T., A., S., and Holben, B.: Multiangle Imaging Spectroradiometer (MISR) global aerosol optical depth validation based on 2 years of coincident Aerosol Robotic Network (AERONET) observations, *J. Geophys. Res.*, 115, 0148–0227, doi:10.1029/2010JD014601, 2010. 25215
- 15 Kaufman, Y. J., Tanré, D., Remer, L. A., Vermote, E. F., Chu, A., and Holben, B. N.: Multiangle Imaging Spectroradiometer (MISR) global aerosol optical depth validation based on 2 years of coincident Aerosol Robotic Network (AERONET) observations, *J. Geophys. Res.*, 102, 17051–17068, doi:10.1029/96JD03988, 1997. 25216
- Kerkweg, A., Buchholz, J., Ganzeveld, L., Pozzer, A., Tost, H., and Jöckel, P.: Technical Note: An implementation of the dry removal processes DRY DEPosition and SEDimentation in the Modular Earth Submodel System (MESSy), *Atmos. Chem. Phys.*, 6, 4617–4632, doi:10.5194/acp-6-4617-2006, 2006a. 25210
- 20 Kerkweg, A., Sander, R., Tost, H., and Jöckel, P.: Technical note: Implementation of prescribed (OFFLEM), calculated (ONLEM), and pseudo-emissions (TNUDGE) of chemical species in the Modular Earth Submodel System (MESSy), *Atmos. Chem. Phys.*, 6, 3603–3609, doi:10.5194/acp-6-3603-2006, 2006b. 25210
- 25 Kettle, A., Andreae, M., Amouroux, D., Andreae, T., Bates, T., Berresheim, H., Bingemer, H., Boniforti, R., Curran, M., DeTullio, G., Helas, G., Jones, G., Keller, M., Kiene, R., Leck, C., Lévassieur, M., Maspero, M., Matraii, P., McTaggart, A., Mihalopoulos, N., Nguyen, B., Novo, A., Putaud, J. P., P., Rapsomanikis, S., Roberts, G., Schebeske, G., Sharma, S., Simo, R., Staubes, R., Turner, S., and Uher, G.: A global database of sea surface dimethylsulfide (DMS) measurements and a simple model to predict sea surface DMS as a function of latitude, longitude and month, *Global Biogeochem. Cy.*, 13, 399–444, 1999. 25214
- 30 Kiehl, J. and Briegleb, B.: The relative roles of sulfate aerosols and greenhouse gases in climate

Aerosol simulation with EMAC

A. Pozzer et al.

Title Page

Abstract

Introduction

Conclusions

References

Tables

Figures

◀

▶

◀

▶

Back

Close

Full Screen / Esc

Printer-friendly Version

Interactive Discussion



forcing, *Science*, 260, 311, 1993. 25217

Klimont, Z., Streets, D., Gupta, S., Cofala, J., Lixin, F., and Ichikawa, Y.: Anthropogenic emissions of non-methane volatile organic compounds in China, *Atmos. Environ.*, 36, 1309–1322, 2002. 25213

5 Lauer, A., Eyring, V., Hendricks, J., Jöckel, P., and Lohmann, U.: Global model simulations of the impact of ocean-going ships on aerosols, clouds, and the radiation budget, *Atmos. Chem. Phys.*, 7, 5061–5079, doi:10.5194/acp-7-5061-2007, 2007. 25211

Lawrence, M. G., Butler, T. M., Steinkamp, J., Gurjar, B. R., and Lelieveld, J.: Regional pollution potentials of megacities and other major population centers, *Atmos. Chem. Phys.*, 7, 3969–3987, doi:10.5194/acp-7-3969-2007, 2007. 25228

10 Lelieveld, J., Brühl, C., Jöckel, P., Steil, B., Crutzen, P. J., Fischer, H., Giorgetta, M. A., Hoor, P., Lawrence, M. G., Sausen, R., and Tost, H.: Stratospheric dryness: model simulations and satellite observations, *Atmos. Chem. Phys.*, 7, 1313–1332, doi:10.5194/acp-7-1313-2007, 2007. 25209

15 Levy, R. C., Remer, L. A., Kleidman, R. G., Mattoo, S., Ichoku, C., Kahn, R., and Eck, T. F.: Global evaluation of the Collection 5 MODIS dark-target aerosol products over land, *Atmos. Chem. Phys.*, 10, 10399–10420, doi:10.5194/acp-10-10399-2010, 2010. 25215

Liu, C., Beirle, S., Butler, T., Liu, J., Hoor, P., Jöckel, P., Pozzer, A., Frankenberg, C., Lawrence, M. G., Lelieveld, J., Platt, U., and Wagner, T.: Application of SCIAMACHY and MOPITT CO total column measurements to evaluate model results over biomass burning regions and Eastern China, *Atmos. Chem. Phys.*, 11, 6083–6114, doi:10.5194/acp-11-6083-2011, 2011. 25218

20 Manders, A. M. M., Schaap, M., Querol, X., Albert, M. F. M. A., Vercauteren, J., Kuhlbusch, T. A. J., and Hoogerbrugge, R.: Sea salt concentrations across the European continent, *Atmos. Environ.*, 44, 2434–2442, doi:10.1016/j.atmosenv.2010.03.028, 2010. 25225

25 Mann, G. W., Carslaw, K. S., Spracklen, D. V., Ridley, D. A., Manktelow, P. T., Chipperfield, M. P., Pickering, S. J., and Johnson, C. E.: Description and evaluation of GLOMAP-mode: a modal global aerosol microphysics model for the UKCA composition-climate model, *Geosci. Model Dev.*, 3, 519–551, doi:10.5194/gmd-3-519-2010, 2010. 25210

30 Maring, H., Savioe, D. L., Izaguirre, M. A., Custals, L., and Reid, J. S.: Vertical distributions of dust and sea-salt aerosols over Puerto Rico during PRIDE measured from a light aircraft, *J. Geophys. Res.*, D19, 8587–8598, doi:10.1029/2002JD002544, 2003. 25226

Mayer, B. and Kylling, A.: Technical note: The libRadtran software package for radiative trans-

Aerosol simulation with EMAC

A. Pozzer et al.

Title Page

Abstract

Introduction

Conclusions

References

Tables

Figures

◀

▶

◀

▶

Back

Close

Full Screen / Esc

Printer-friendly Version

Interactive Discussion



fer calculations – description and examples of use, *Atmos. Chem. Phys.*, 5, 1855–1877, doi:10.5194/acp-5-1855-2005, 2005. 25211

McInnes, L. M., Covert, D. S., Quinn, P. K., and Germani, M. S.: Measurements of chloride depletion and sulfur enrichment in individual sea-salt particles collected from the remote marine boundary layer, *J. Geophys. Res.*, 99, 8257–8268, doi:10.1029/93JD03453, 1994. 25225

de Meij, A., Krol, M., Dentener, F., Vignati, E., Cuvelier, C., and Thunis, P.: The sensitivity of aerosol in Europe to two different emission inventories and temporal distribution of emissions, *Atmos. Chem. Phys.*, 6, 4287–4309, doi:10.5194/acp-6-4287-2006, 2006. 25208, 25213, 25220, 25223, 25230

Millero, F. J.: Physicochemical controls on seawater, *Treatise Geochem.*, 6, 1–21, 2003. 25225

Myhre, G., Grini, A., and Metzger, S.: Modelling of nitrate and ammonium-containing aerosols in presence of sea salt, *Atmos. Chem. Phys.*, 6, 4809–4821, doi:10.5194/acp-6-4809-2006, 2006. 25208

Nenes, A., Pandis, S. N., and Pilinis, C.: ISORROPIA: a new thermodynamic equilibrium model for multiphase multicomponent inorganic aerosols, *Aquat. Geochem.*, 1, 123–152, doi:10.1023/A:1009604003981, 1998a. 25211

Nenes, A., Pandis, S. N., and Pilinis, C.: Continued development and testing of a new thermodynamic aerosol module for urban and regional air quality models, *Atmos. Environ.*, 33, 1553–1560, 1998b. 25211

Ohara, T., Akimoto, H., Kurokawa, J., Horii, N., Yamaji, K., Yan, X., and Hayaşaka, T.: An Asian emission inventory of anthropogenic emission sources for the period 1980–2013, *Atmos. Chem. Phys.*, 7, 4419–4444, doi:10.5194/acp-7-4419-2007, 2007. 25213, 25228

Olivier, J. G. J., Bouwman, A. F., van der Maas, C. W. M., Berdowski, J. J. M., Veldt, C., Bloos, J. P. J., Visschedijk, A. J. J., Zandveld, P. Y. J., and Haverlag, J. L.: Description of EDGAR Version 2.0: a set of global inventories of greenhouse gases and ozone-depleting substances for all anthropogenic and most natural sources on a per country $1^\circ \times 1^\circ$ grid, RIVM Rep. 771060002, Rijksinstituut, Bilthoven, Netherlands, 1996. 25208

Olivier, J. G. J., Bloos, J. P. J., Berdowski, J. J. M., Visschedijk, A. J. H., and Bouwman, A. F.: A 1990 global emission inventory of anthropogenic sources of carbon monoxide on $1^\circ \times 1^\circ$ developed in the framework of EDGAR/GEIA, *Chemosphere*, 1, 1–17, 1999. 25208

Olson, J.: World Ecosystems (WE1.4): Digital Raster Data on a 10 min Geographic 1080 × 2160 Grid Square, Global Ecosystem Database, ISBN:92-63-02182-1, NOAA, pub-

- lisher, National Geophysical Data Center, location: Boulder, Colorado, 1992. 25214
- Pinder, R. W., Strader, R., Davidson, C. I., and Adams, P. J.: A temporally and spatially resolved ammonia emission inventory for dairy cows in the United States, *Atmos. Environ.*, 38, 3747–3756, doi:10.1016/j.atmosenv.2004.04.008, <http://www.sciencedirect.com/science/article/B6VH3-4CGMX5D-2/2/220d75c6628a232740644f696f9a9441>, 2004. 25208
- Pozzer, A., Jöckel, P., Sander, R., Williams, J., Ganzeveld, L., and Lelieveld, J.: Technical Note: The MESSy-submodel AIRSEA calculating the air-sea exchange of chemical species, *Atmos. Chem. Phys.*, 6, 5435–5444, doi:10.5194/acp-6-5435-2006, 2006. 25210, 25214
- Pozzer, A., Jöckel, P., Tost, H., Sander, R., Ganzeveld, L., Kerkweg, A., and Lelieveld, J.: Simulating organic species with the global atmospheric chemistry general circulation model ECHAM5/MESSy1: a comparison of model results with observations, *Atmos. Chem. Phys.*, 7, 2527–2550, doi:10.5194/acp-7-2527-2007, 2007. 25209
- Pozzer, A., Jöckel, P., and Van Aardenne, J.: The influence of the vertical distribution of emissions on tropospheric chemistry, *Atmos. Chem. Phys.*, 9, 9417–9432, doi:10.5194/acp-9-9417-2009, 2009. 25213
- Price, C. and Rind, D.: A simple lightning parameterization for calculating global lightning distributions, *J. Geophys. Res.*, 97, 9919–9933, 1992. 25213
- Pringle, K. J., Tost, H., Message, S., Steil, B., Giannadaki, D., Nenes, A., Fountoukis, C., Stier, P., Vignati, E., and Lelieveld, J.: Description and evaluation of GMXe: a new aerosol submodel for global simulations (v1), *Geosci. Model Dev.*, 3, 391–412, doi:10.5194/gmd-3-391-2010, 2010a. 25208, 25210, 25214, 25217, 25225, 25226, 25227
- Pringle, K. J., Tost, H., Pozzer, A., Pöschl, U., and Lelieveld, J.: Global distribution of the effective aerosol hygroscopicity parameter for CCN activation, *Atmos. Chem. Phys.*, 10, 5241–5255, doi:10.5194/acp-10-5241-2010, 2010b. 25210, 25211
- Pye, H., Liao, H., Wu, S., Mickley, L., Jacob, D., Henze, D., and Seinfeld, J.: Effect of changes in climate and emissions on future sulfate-nitrate-ammonium aerosol levels in the United States, *J. Geophys. Res.*, 114, 1–18, 2009. 25227
- Ramanathan, V., Crutzen, P., Kiehl, J., and Rosenfeld, D.: Aerosols, climate, and the hydrological cycle, *Science*, 294, 2119, 2001. 25207
- Remer, L., Kleidman, R., Levy, R., Kaufman, Y., Tanré, D., Mattoo, S., Martins, J., Ichoku, C., Koren, I., Yu, H., and Holben, B. H.: Global aerosol climatology from the MODIS satellite sensors, *J. Geophys. Res.*, 113, D14S07, doi:10.1029/2007JD009661, 2008. 25215
- Rodriguez, M. and Dabdub, D.: IMAGES-SCAPE2: a modeling study of size-and chemically

**Aerosol simulation
with EMAC**

A. Pozzer et al.

Title Page

Abstract

Introduction

Conclusions

References

Tables

Figures

◀

▶

◀

▶

Back

Close

Full Screen / Esc

Printer-friendly Version

Interactive Discussion



- resolved aerosol thermodynamics in a global chemical transport model, *J. Geophys. Res.*, 109, D02203, doi:10.1029/2003JD003639, 2004. 25227
- Roeckner, E., Brokopf, R., Esch, M., Giorgetta, M., Hagemann, S., Kornblueh, L., Manzini, E., Schlese, U., and Schulzweida, U.: Sensitivity of simulated climate to horizontal and vertical resolution in the ECHAM5 atmosphere model, *J. Climate*, 19, 3771–3791, 2006. 25209
- Sander, R., Kerkweg, A., Jöckel, P., and Lelieveld, J.: Technical note: The new comprehensive atmospheric chemistry module MECCA, *Atmos. Chem. Phys.*, 5, 445–450, doi:10.5194/acp-5-445-2005, 2005. 25210
- Schaap, M.: On the importance of aerosol nitrate in Europe, Data analysis and modelling, Ph.D. thesis, University of Utrecht, <http://www.library.uu.nl/digiarchief/dip/diss/2003-1209-110044/inhoud.htm>, 2003. 25223
- Schaap, M., van Loon, M., ten Brink, H. M., Dentener, F. J., and Builtjes, P. J. H.: Secondary inorganic aerosol simulations for Europe with special attention to nitrate, *Atmos. Chem. Phys.*, 4, 857–874, doi:10.5194/acp-4-857-2004, 2004. 25223, 25230
- Shettle, E.: Models for the Aerosols of the Lower Atmosphere and the Effects of Humidity Variations on their Optical Properties, Tech. Rep. ADA085951, Air Force Geophysics Lab, Hanscom AFB MA, 1979. 25211
- Simpson, D., Fagerli, H., Jonson, J., Tsyro, S., Wind, P., and Tuovinen, J.-P.: Transboundary acidification and eutrophication and ground level ozone in Europe: Unified EMEP Model Description., Tech. rep., Norwegian Meteorological Institute, Oslo, Norway, 2003. 25213
- Stier, P., Feichter, J., Kinne, S., Kloster, S., Vignati, E., Wilson, J., Ganzeveld, L., Tegen, I., Werner, M., Balkanski, Y., Schulz, M., Boucher, O., Minikin, A., and Petzold, A.: The aerosol-climate model ECHAM5-HAM, *Atmos. Chem. Phys.*, 5, 1125–1156, doi:10.5194/acp-5-1125-2005, 2005. 25210, 25226
- Streets, D. and Waldhoff, S.: Present and future emissions of air pollutants in China: SO₂, NO_x, and CO, *Atmos. Environ.*, 34, 363–374, 2000. 25228
- Streets, D., Bond, T. C., Carmichael, G. R., Fernandes, S. D., Fu, Q., He, D., Klimont, Z., Nelson, S. M., Tsai, N. Y., Wang, M. Q., Woo, J. H., and Yarber, K. F.: An inventory of gaseous and primary aerosol emission in Asia in the year 2000, *J. Geophys. Res.*, 108, 8809, doi:10.1029/2002JD003093, 2003. 25213, 25228
- Sutherland, R. and Khanna, R.: Optical properties of organic-based aerosols produced by burning vegetation, *Aerosol Sci. Tech.*, 14, 331–342, 1991. 25211
- Tanré, D., Kaufman, Y. J., Herman, M., and Mattoo, S.: Multiangle Imaging Spectro-

**Aerosol simulation
with EMAC**

A. Pozzer et al.

Title Page

Abstract

Introduction

Conclusions

References

Tables

Figures

◀

▶

◀

▶

Back

Close

Full Screen / Esc

Printer-friendly Version

Interactive Discussion



Aerosol simulation with EMAC

A. Pozzer et al.

Title Page

Abstract

Introduction

Conclusions

References

Tables

Figures

◀

▶

◀

▶

Back

Close

Full Screen / Esc

Printer-friendly Version

Interactive Discussion



diometer (MISR) global aerosol optical depth validation based on 2 years of coincident Aerosol Robotic Network (AERONET) observations, *J. Geophys. Res.*, 102, 16971–16988, doi:10.1029/96JD03437, 1997. 25216

Taylor, K.: Summarizing multiple aspects of model performance in a single diagram, *J. Geophys. Res.*, 106, 7183–7192, 2001. 25219

Textor, C., Schulz, M., Guibert, S., Kinne, S., Balkanski, Y., Bauer, S., Berntsen, T., Berglen, T., Boucher, O., Chin, M., Dentener, F., Diehl, T., Easter, R., Feichter, H., Fillmore, D., Ghan, S., Ginoux, P., Gong, S., Grini, A., Hendricks, J., Horowitz, L., Huang, P., Isaksen, I., Iversen, I., Kloster, S., Koch, D., Kirkevåg, A., Kristjansson, J. E., Krol, M., Lauer, A., Lamarque, J. F., Liu, X., Montanaro, V., Myhre, G., Penner, J., Pitari, G., Reddy, S., Seland, Ø., Stier, P., Takemura, T., and Tie, X.: Analysis and quantification of the diversities of aerosol life cycles within AeroCom, *Atmos. Chem. Phys.*, 6, 1777–1813, doi:10.5194/acp-6-1777-2006, 2006. 25207, 25226

Tost, H., Jöckel, P., Kerkweg, A., Sander, R., and Lelieveld, J.: Technical note: A new comprehensive SCAVenging submodel for global atmospheric chemistry modelling, *Atmos. Chem. Phys.*, 6, 565–574, doi:10.5194/acp-6-565-2006, 2006a. 25210

Tost, H., Jöckel, P., and Lelieveld, J.: Influence of different convection parameterisations in a GCM, *Atmos. Chem. Phys.*, 6, 5475–5493, doi:10.5194/acp-6-5475-2006, 2006b. 25210

Tost, H., Jöckel, P., Kerkweg, A., Pozzer, A., Sander, R., and Lelieveld, J.: Global cloud and precipitation chemistry and wet deposition: tropospheric model simulations with ECHAM5/MESSy1, *Atmos. Chem. Phys.*, 7, 2733–2757, doi:10.5194/acp-7-2733-2007, 2007a. 25210

Tost, H., Jöckel, P., and Lelieveld, J.: Lightning and convection parameterisations – uncertainties in global modelling, *Atmos. Chem. Phys.*, 7, 4553–4568, doi:10.5194/acp-7-4553-2007, 2007b. 25210

UNECE/UNFCCC National Communication United Nations Framework Convention on Climate Change, <http://unfccc.int>, 2008. 25213

Vestreng, V. and Klein, H.: Emission data reported to UNECE/EMEP: quality assurance and trend analysis and presentation of WebDab, MSC-W Status Rep. 2002, Norw. Meteorol. Inst., Oslo, Norway, 2002. 25213

Vestreng, V., Myhre, G., Fagerli, H., Reis, S., and Tarrasón, L.: Twenty-five years of continuous sulphur dioxide emission reduction in Europe, *Atmos. Chem. Phys.*, 7, 3663–3681, doi:10.5194/acp-7-3663-2007, 2007. 25227

**Aerosol simulation
with EMAC**

A. Pozzer et al.

Title Page

Abstract

Introduction

Conclusions

References

Tables

Figures

◀

▶

◀

▶

Back

Close

Full Screen / Esc

Printer-friendly Version

Interactive Discussion



- Vestreng, V., Ntziachristos, L., Semb, A., Reis, S., Isaksen, I. S. A., and Tarrasón, L.: Evolution of NO_x emissions in Europe with focus on road transport control measures, *Atmos. Chem. Phys.*, 9, 1503–1520, doi:10.5194/acp-9-1503-2009, 2009. 25227
- 5 Vignati, E., Wilson, J., and Stier, P.: M7: an efficient size-resolved aerosol micro-physics module for large-scale aerosol transport models, *J. Geophys. Res.*, 109, D22202, doi:10.1029/2003JD004485, 2004. 25210
- Wanninkhof, R.: Relationship between wind speed and gas exchange over the ocean, *J. Geophys. Res.*, 97, 7373–7382, 1992. 25214
- 10 van der Werf, G. R., Randerson, J. T., Giglio, L., Collatz, G. J., Mu, M., Kasibhatla, P. S., Morton, D. C., DeFries, R. S., Jin, Y., and van Leeuwen, T. T.: Global fire emissions and the contribution of deforestation, savanna, forest, agricultural, and peat fires (1997–2009), *Atmos. Chem. Phys.*, 10, 11707–11735, doi:10.5194/acp-10-11707-2010, 2010. 25214, 25244, 25245
- White, W. H.: Chemical markers for sea salt in IMPROVE aerosol data, *Atmos. Environ.*, 15 42, 261–274, doi:10.1016/j.atmosenv.2007.09.040, <http://www.sciencedirect.com/science/article/B6VH3-4PPMXW7-9/2/91363e441efaf95eb2e254c6e82a2d8e>, 2008. 25225
- Yienger, J. J. and Levy, H.: Empirical model of global soil-biogenic NO_x emissions, *J. Geophys. Res.*, 100, 11447–11464, 1995. 25214
- 20 Zhang, Q., Streets, D. G., Carmichael, G. R., He, K. B., Huo, H., Kannari, A., Klimont, Z., Park, I. S., Reddy, S., Fu, J. S., Chen, D., Duan, L., Lei, Y., Wang, L. T., and Yao, Z. L.: Asian emissions in 2006 for the NASA INTEX-B mission, *Atmos. Chem. Phys.*, 9, 5131–5153, doi:10.5194/acp-9-5131-2009, 2009. 25230

Table 1. Global gas emissions for the year 2005. In bold are the emissions calculated on-line by the submodels ONLEM or AIRSEA (maximum and minimum).

Trace gas	Anthropogenic ^a	Biomass burning ^b	Natural	Total
CO	584.1	356.8	112.4	1053.3
C ₂ H ₄	6.9	3.6	11.3	21.8
C ₂ H ₆	7.5	2.0	0.5	10.1
C ₃ H ₆	3.0	1.6	3.4	8.0
C ₃ H ₈	9.0	0.6	0.3	10.0
C ₄ H ₁₀ ^c	63.0	0.8	0.4	64.2
MEK ^d	7.0	3.1	–	8.2
CH ₃ CHO	1.5	1.4	–	2.9
CH ₃ COCH ₃	4.1	1.3	55.6	61.0
CH ₃ COOH	4.8	4.6	3.4	12.7
CH ₃ OH	7.6	4.6	150.1	162.3
HCHO	3.4	2.4	–	5.9
HCOOH	2.6	2.5	5.6	10.7
SO ₂	140.4	2.3	29.1	171.9
NH ₃	40.7	–	10.6	51.3
DMS	–	–	44.6–45.6	45.3
ISOPRENE	–	–	394.9–420.8	408.0
NO _x ^e	27.9	4.6	7.7–8.6	41.0

^a Based on the CIRCE-EDGAR inventory for the year 2005.

^b From GFEDv3.1 (van der Werf et al., 2010), averaged over the years 1997–2009.

^c It includes higher alkanes.

^d Methyl ethyl ketone plus all higher ketones.

^e In unit of Tg N yr⁻¹. The natural emissions include soil and lightning source.

**Aerosol simulation
with EMAC**

A. Pozzer et al.

Title Page

Abstract

Introduction

Conclusions

References

Tables

Figures

◀

▶

◀

▶

Back

Close

Full Screen / Esc

Printer-friendly Version

Interactive Discussion



Aerosol simulation with EMAC

A. Pozzer et al.

Title Page

Abstract

Introduction

Conclusions

References

Tables

Figures

◀

▶

◀

▶

Back

Close

Full Screen / Esc

Printer-friendly Version

Interactive Discussion



Table 2. Global aerosol emissions for the year 2005.

Aerosol	Anthropogenic ^a	Biomass burning ^b	Natural ^c	Total
BC	6.0	2.1	–	8.1
POM	18.8	25.8	19.1	63.7
DU	–	–	1669.8	1669.8
SS	–	–	7888.3	7888.3

^a From based on the CIRCE-EDGAR inventory, for the year 2005.

^b From GFEDv3.1 (van der Werf et al., 2010), averaged over the year 1997–2009.

^c From AEROCOM (Dentener et al., 2006).

Aerosol simulation with EMAC

A. Pozzer et al.

Table 3. Summary of the comparison of model data to observations of aerosol concentrations. OAM and MAM are the arithmetic mean of the observations and of the model, respectively (in $\mu\text{g m}^{-3}$). The model has been sampled at the locations of the observations, and the average corresponds to the 2005–2008 period. PF2 is the percentage of modelled point within a factor of two of the observations.

Species	Network	MAM	OAM	MAM/OAM	PF2
SO_4^{2-}	CASTNET	2.1	2.9	0.7	95.3
SO_4^{2-}	EMEP	1.6	1.9	0.8	92.3
SO_4^{2-}	EANET	2.4	4.4	0.5	88.7
NO_3^-	CASTNET	1.7	0.9	1.9	46.0
NO_3^-	EMEP	2.5	1.6	1.6	64.5
NO_3^-	EANET	1.9	1.2	1.6	52.0
NH_4^+	CASTNET	1.0	1.0	1.0	87.7
NH_4^+	EMEP	1.2	0.9	1.3	80.6
NH_4^+	EANET	0.9	1.1	0.8	81.9
Na^+	CASTNET	0.3	0.1	3.2	49.8
Na^+	EMEP	3.5	0.9	3.9	15.7
Na^+	EANET	2.9	1.0	2.8	33.8

[Title Page](#)
[Abstract](#)
[Introduction](#)
[Conclusions](#)
[References](#)
[Tables](#)
[Figures](#)
[I◀](#)
[▶I](#)
[◀](#)
[▶](#)
[Back](#)
[Close](#)
[Full Screen / Esc](#)
[Printer-friendly Version](#)
[Interactive Discussion](#)


Aerosol simulation with EMAC

A. Pozzer et al.

Table 4. Global aerosol budget. All units in Tg (species) yr⁻¹, except nitrogen and sulfur compounds (expressed as Tg N yr⁻¹ and Tg S yr⁻¹, respectively). NO_y includes NO, NO₂, peroxyacetyl nitrate (PAN), NO₃, HNO₄ and N₂O₅, and not nitric acid or aerosol nitrate. SO_x includes SO₂, H₂SO₄ and DMS, and not aerosol sulfate. The yearly standard deviation is listed in parenthesis.

	Emissions		Dry deposition		Sedimentation		Wet deposition		Burden	
DU	1659.3	(12.6)	65.3	(3.1)	1183.5	(18.5)	403.3	(11.1)	10.6	(0.3)
SS	7843.9	(50.0)	1422.8	(25.7)	4090.7	(13.4)	2314.3	(13.5)	5.8	(0.3)
BC	8.1	(0.1)	0.8	(0.0)	0.8	(0.0)	6.2	(0.1)	0.1	(0.0)
POM	63.4	(0.5)	6.1	(0.1)	6.1	(0.1)	50.0	(0.6)	1.0	(0.0)
NH ₃	41.0	(0.2)	16.3	(0.1)	–		–		0.1	(0.0)
NH ₄ ⁺	–		0.9	(0.0)	2.6	(0.1)	21.0	(0.2)	0.1	(0.0)
SO _x	108.1	(0.9)	26.0	(0.2)	–		–		0.6	(0.0)
SO ₄ ²⁻	2.1	(0.0)	6.2	(0.1)	23.8	(0.2)	55.0	(0.5)	0.3	(0.0)
NO _y	40.0	(0.2)	4.4	(0.0)	–		–		2.0	(0.1)
HNO ₃	–		9.8	(0.1)	–		–		1.1	(0.0)
NO ₃ ⁻	–		1.0	(0.0)	6.7	(0.1)	18.9	(0.2)	0.1	(0.0)

[Title Page](#)
[Abstract](#)
[Introduction](#)
[Conclusions](#)
[References](#)
[Tables](#)
[Figures](#)
[I◀](#)
[▶I](#)
[◀](#)
[▶](#)
[Back](#)
[Close](#)
[Full Screen / Esc](#)
[Printer-friendly Version](#)
[Interactive Discussion](#)


Table 5. Regional aerosol budgets. All units in Gg(species) yr⁻¹, except nitrogen and sulfur compounds (expressed as Gg N yr⁻¹ and Gg S yr⁻¹, respectively) and the species are as in Table 4. The transport is positive (negative) associated with a net import (export) to (from) the region. The yearly standard deviation is listed in parenthesis.

	Emissions	Dry deposition	Sedimentation	Wet deposition	Transport	Burden
North America (26° W–72° W and 30° N–52° N)						
DU	7505.0 (63.8)	622.1 (38.4)	4563.7 (72.94)	1707.5 (89.1)	-385.6 (83.4)	32.1 (1.1)
SS	21524.3 (221.7)	2613.1 (149.9)	13551.4 (313.84)	6852.2 (243.1)	987.0 (342.2)	29.2 (1.7)
BC	511.7 (4.7)	59.7 (1.1)	17.7 (0.79)	223.5 (4.3)	-198.9 (7.2)	4.8 (0.2)
POM	1986.2 (84.6)	248.5 (9.6)	64.3 (4.17)	1010.7 (35.7)	-489.2 (72.3)	22.3 (1.6)
NH ₃	2972.8 (11.6)	960.2 (18.8)	–	0.0 (0.0)	-35.7 (21.6)	7.9 (0.3)
NH ₄ ⁺	–	131.6 (4.9)	219.4 (16.03)	1251.8 (23.0)	-303.8 (11.6)	8.4 (0.3)
SO _x	7336.4 (63.3)	1776.5 (43.9)	–	–	-1216.9 (111.0)	33.4 (0.3)
SO ₄ ²⁻	181.3 (1.3)	237.2 (10.9)	469.2 (22.80)	2904.9 (71.8)	-486.1 (23.4)	13.2 (0.5)
NO _x	5699.4 (38.3)	582.7 (21.4)	–	–	-987.7 (160.4)	66.3 (1.7)
HNO ₃	–	1703.8 (19.9)	–	2.6 (0.4)	-625.0 (97.4)	35.2 (0.5)
NO ₃ ⁻	–	56.4 (2.6)	197.2 (5.00)	1242.5 (17.8)	-59.7 (7.9)	2.2 (0.1)
Europe (12° W–36° E and 34° N–62° N)						
DU	4459.9 (18.8)	1856.4 (168.7)	11210.7 (823.2)	30349.2 (2234.5)	34617.6 (3581.8)	386.0 (29.0)
SS	85557.5 (912.9)	14540.0 (517.8)	46657.7 (1078.2)	28457.0 (1406.6)	2007.0 (670.2)	80.8 (2.0)
BC	662.0 (5.5)	76.6 (1.0)	53.3 (2.2)	290.5 (5.6)	-224.7 (7.5)	5.4 (0.1)
POM	1091.9 (26.6)	136.9 (3.3)	96.6 (3.0)	568.8 (24.8)	-214.2 (25.5)	12.2 (0.5)
NH ₃	5261.0 (19.3)	2122.8 (42.6)	–	0.2 (0.0)	-147.0 (7.5)	7.8 (0.4)
NH ₄ ⁺	–	197.1 (4.4)	391.8 (37.5)	2008.6 (78.6)	-271.1 (8.9)	8.9 (0.5)
SO _x	11232.3 (92.2)	3530.3 (37.7)	–	–	-1884.6 (119.4)	45.5 (0.7)
SO ₄ ²⁻	273.8 (1.9)	320.3 (3.2)	917.5 (38.2)	3620.3 (47.9)	-607.5 (26.0)	16.4 (0.7)
NO _x	5058.4 (32.5)	634.5 (11.2)	–	–	-576.4 (180.6)	68.8 (1.6)
HNO ₃	–	920.9 (17.4)	–	–	-415.6 (120.4)	36.7 (0.7)
NO ₃ ⁻	–	150.9 (5.0)	597.2 (25.6)	1394.2 (40.2)	-115.1 (7.2)	3.7 (0.1)
East Asia (100° E–144° E and 20° N–44° N)						
DU	45933.8 (309.1)	3294.9 (116.1)	37822.6 (986.7)	16845.0 (800.4)	10354.2 (1099.9)	351.4 (11.2)
SS	89937.5 (886.3)	7016.6 (421.5)	48863.3 (1272.1)	30749.6 (730.0)	-4424.2 (619.9)	96.3 (4.5)
BC	1476.6 (15.2)	133.9 (0.8)	140.5 (5.7)	972.2 (26.7)	-159.8 (23.3)	15.3 (0.3)
POM	6263.3 (70.1)	594.6 (7.9)	612.3 (12.9)	4976.6 (198.7)	201.3 (142.7)	77.0 (2.5)
NH ₃	6097.2 (23.1)	1868.5 (13.5)	–	0.1 (0.0)	501.4 (61.5)	12.8 (0.3)
NH ₄ ⁺	–	244.9 (7.1)	580.3 (23.5)	3563.1 (75.5)	-226.7 (45.4)	20.7 (0.4)
SO _x	23935.0 (201.6)	7715.1 (96.0)	–	–	-2187.1 (186.2)	93.7 (1.8)
SO ₄ ²⁻	591.2 (4.3)	502.4 (15.5)	1790.9 (38.2)	10413.7 (140.4)	-889.2 (59.9)	31.8 (0.8)
NO _x	7262.6 (49.2)	645.1 (9.2)	–	–	-568.3 (163.4)	66.0 (1.5)
HNO ₃	–	1407.8 (29.3)	–	1.2 (0.1)	-330.1 (140.0)	34.9 (1.0)
NO ₃ ⁻	–	121.1 (5.6)	594.0 (12.9)	3028.7 (48.1)	-164.5 (17.4)	7.0 (0.2)
Central Africa (10° E–40° E and 10° S–10° N)						
DU	3.5 (0.3)	3762.6 (552.4)	9418.7 (986.7)	24017.1 (1431.9)	33347.4 (2650.8)	327.2 (43.6)
SS	713.3 (5.2)	321.1 (5.5)	1245.0 (8.1)	1470.5 (70.9)	2182.6 (88.6)	17.8 (0.6)
BC	838.7 (31.8)	78.1 (1.3)	32.3 (1.6)	597.8 (42.7)	-92.3 (23.5)	13.0 (0.5)
POM	8928.1 (324.2)	870.3 (14.5)	543.2 (29.0)	5990.5 (422.4)	-1079.8 (228.2)	119.0 (4.3)
NH ₃	761.8 (4.9)	256.8 (16.3)	–	0.0 (0.0)	116.1 (11.2)	3.8 (0.3)
NH ₄ ⁺	–	8.6 (0.5)	14.8 (1.0)	646.4 (19.7)	31.0 (7.9)	1.9 (0.1)
SO _x	708.6 (15.2)	160.5 (8.1)	–	–	230.7 (15.2)	4.8 (0.2)
SO ₄ ²⁻	18.5 (0.4)	36.9 (1.5)	80.7 (2.9)	768.8 (34.8)	87.5 (16.1)	5.4 (0.3)
NO _x	2115.7 (68.1)	203.8 (13.5)	–	–	-361.7 (139.8)	35.2 (1.5)
HNO ₃	–	670.9 (8.5)	–	0.1 (0.0)	-62.2 (7.8)	16.2 (0.8)
NO ₃ ⁻	–	9.1 (0.5)	24.2 (1.8)	692.0 (65.6)	56.8 (4.5)	0.7 (0.0)
South America (75° W–35° W and 30° S–0° N)						
DU	3382.4 (15.4)	472.7 (61.1)	2218.3 (32.5)	4630.4 (563.7)	3422.3 (577.9)	38.0 (4.0)
SS	30004.4 (163.4)	3230.5 (150.5)	22772.9 (196.4)	11909.4 (590.2)	6823.9 (599.2)	68.9 (1.6)
BC	599.4 (103.2)	64.3 (11.8)	21.6 (6.3)	319.7 (65.6)	-154.0 (24.2)	8.1 (1.7)
POM	10020.4 (1144.5)	1012.7 (129.3)	339.8 (96.2)	5603.7 (898.4)	-2484.2 (341.9)	117.5 (15.8)
NH ₃	2606.4 (16.7)	1110.2 (14.9)	–	–	-73.4 (32.7)	7.7 (1.0)
NH ₄ ⁺	–	15.3 (1.7)	29.0 (3.1)	1252.2 (56.0)	-77.7 (13.3)	2.3 (0.2)
SO _x	3827.7 (60.7)	625.5 (6.8)	–	–	-703.6 (117.8)	20.9 (0.2)
SO ₄ ²⁻	91.2 (1.4)	84.3 (5.2)	309.9 (10.6)	1582.8 (123.2)	-245.2 (27.3)	9.7 (0.6)
NO _x	2576.2 (210.0)	320.0 (19.4)	–	–	-807.9 (170.9)	62.6 (2.9)
HNO ₃	–	467.8 (102.1)	–	0.2 (0.0)	-89.6 (134.7)	22.1 (1.5)
NO ₃ ⁻	–	29.3 (2.3)	86.7 (3.5)	534.3 (79.2)	62.5 (6.8)	1.5 (0.1)

Aerosol simulation with EMAC

A. Pozzer et al.

Title Page

Abstract

Introduction

Conclusions

References

Tables

Figures

⏪

⏩

⏴

⏵

Back

Close

Full Screen / Esc

Printer-friendly Version

Interactive Discussion



Aerosol simulation with EMAC

A. Pozzer et al.

Table 6. Comparison of model results to observations of aerosol concentrations. OAM and MAM are the arithmetic mean of the observations and of the model, respectively (in $\mu\text{g m}^{-3}$). Bias represents the difference between MAM and OAM. The model has been sampled at the locations of the observations, and the average corresponds to the 2005 period. PF2 is the percentage of modelled concentrations within a factor of two of the observations.

Species	Network	OAM	MAM	ST Bias	PF2	MAM	NS Bias	PF2	PF2 difference PF2(ST) – PF2(NS)
SO ₄ ²⁻	CASTNET	2.9	2.0	-0.8	94.7	2.2	-0.6	94.2	0.5
SO ₄ ²⁻	EMEP	1.9	1.6	-0.5	94.0	1.7	-0.4	92.7	1.3
SO ₄ ²⁻	EANET	4.4	2.4	-2.1	92.3	2.4	-2.1	91.7	0.6
NO ₃ ⁻	CASTNET	0.9	1.7	0.9	42.6	1.9	1.1	40.1	2.5
NO ₃ ⁻	EMEP	1.6	2.7	1.0	66.1	2.7	1.0	66.1	0.0
NO ₃ ⁻	EANET	1.2	1.9	0.7	52.5	1.9	0.7	53.1	-0.6
NH ₄ ⁺	CASTNET	1.0	1.0	0.0	86.8	1.1	0.1	83.2	3.6
NH ₄ ⁺	EMEP	0.9	1.3	0.2	82.7	1.4	0.3	78.4	4.3
NH ₄ ⁺	EANET	1.1	0.9	-0.2	86.1	0.9	-0.2	85.1	0.9
Na ⁺	CASTNET	0.1	0.3	0.2	43.4	0.3	0.2	42.6	0.8
Na ⁺	EMEP	0.9	3.6	2.6	13.5	3.7	2.7	13.5	0.0
Na ⁺	EANET	1.0	2.9	1.9	36.3	2.9	1.9	36.0	0.3

Title Page

Abstract

Introduction

Conclusions

References

Tables

Figures

◀

▶

◀

▶

Back

Close

Full Screen / Esc

Printer-friendly Version

Interactive Discussion



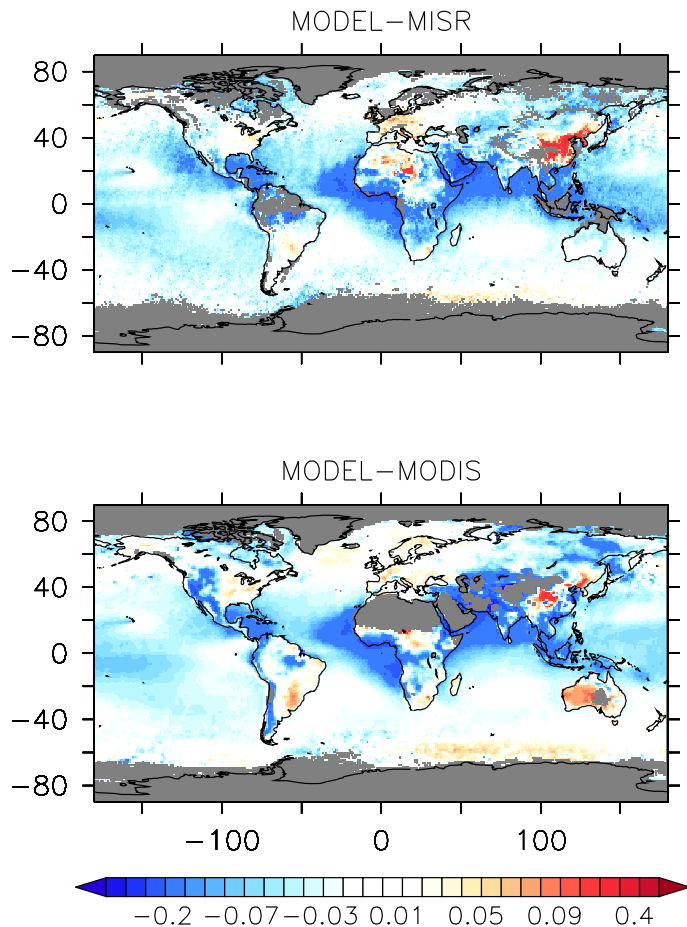


Fig. 1. Annual average AOD difference between model results and MODIS and MISR observations (level 3 product). In grey the regions with less than 12 observations present during the years 2005–2008.

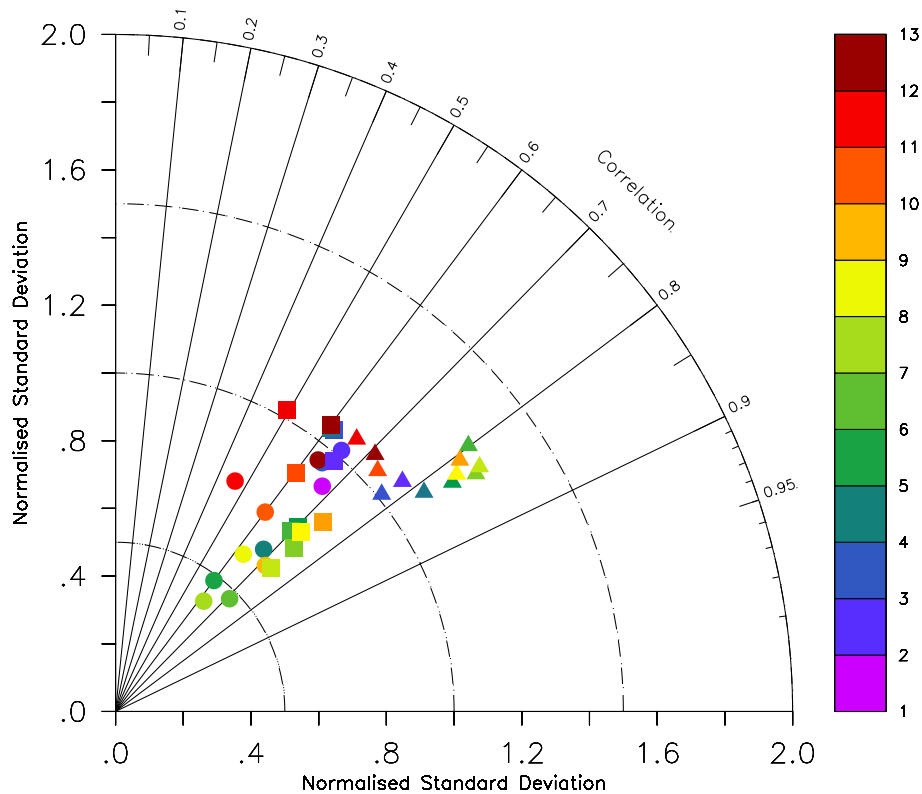


Fig. 2. Taylor diagram of the comparisons between satellite observations and model results of AOD. The comparison with MODIS and MISR are depicted with squares and circles, respectively. The triangles denote the comparison between MISR and MODIS observations. The color code denotes the month of the year.

Aerosol simulation with EMAC

A. Pozzer et al.

Title Page

Abstract Introduction

Conclusions References

Tables Figures

◀ ▶

◀ ▶

Back Close

Full Screen / Esc

Printer-friendly Version

Interactive Discussion



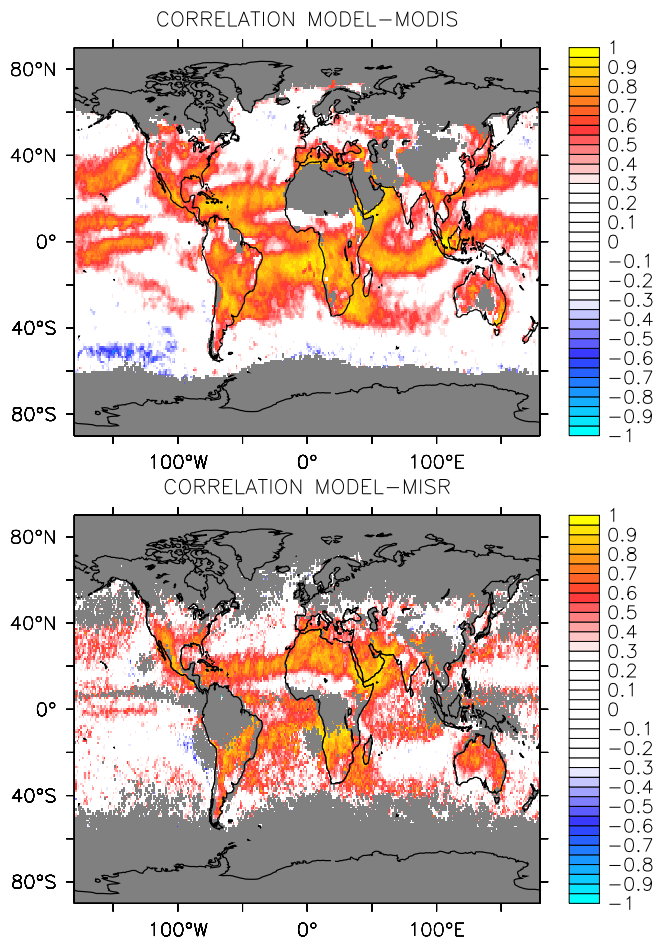


Fig. 3. Correlation (R) between model results and MODIS and MISR observations (level 3 product) of AOD. In grey the regions with less than 24 observations/months present during the years 2005–2008.

**Aerosol simulation
with EMAC**

A. Pozzer et al.

Title Page

Abstract Introduction

Conclusions References

Tables Figures

◀ ▶

◀ ▶

Back Close

Full Screen / Esc

Printer-friendly Version

Interactive Discussion



Aerosol simulation
with EMAC

A. Pozzer et al.

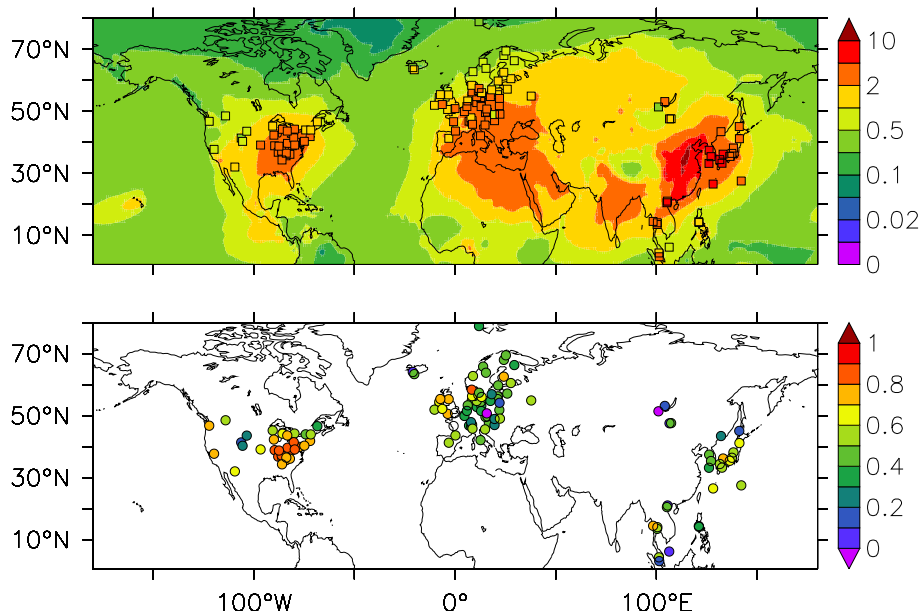


Fig. 4. UPPER: simulated mean concentrations of SO_4^{2-} (in $\mu\text{g m}^{-3}$) for the year 2005–2008, with observations from CASTNET, EMEP and EANET (averaged over the same period) overplotted. LOWER: temporal correlation of observations from CASTNET, EMEP and EANET and model results for SO_4^{2-} .

[Title Page](#)[Abstract](#)[Introduction](#)[Conclusions](#)[References](#)[Tables](#)[Figures](#)[◀](#)[▶](#)[◀](#)[▶](#)[Back](#)[Close](#)[Full Screen / Esc](#)[Printer-friendly Version](#)[Interactive Discussion](#)

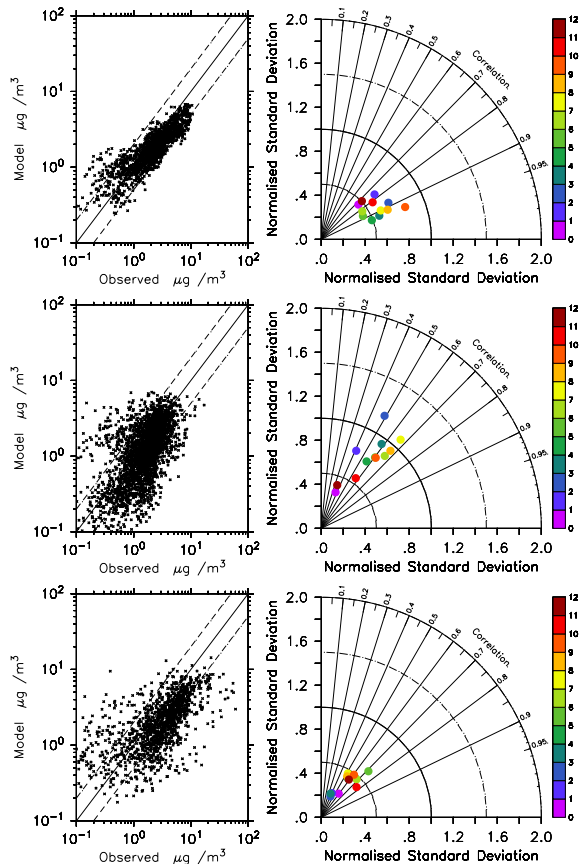


Fig. 5. LEFT: Scatter plots of observed and modelled monthly averaged concentrations (in $\mu\text{g m}^{-3}$) for the year 2005–2008 of SO_4^{2-} . RIGHT: Taylor diagram of the comparison between station observations and model results. The color code denotes the month of the year for which the statistical values are calculated. UPPER: observations from CASTNET, MIDDLE: observations from EMEP, LOWER: observations from EANET.

Aerosol simulation with EMAC

A. Pozzer et al.

Title Page

Abstract Introduction

Conclusions References

Tables Figures

◀ ▶

◀ ▶

Back Close

Full Screen / Esc

Printer-friendly Version

Interactive Discussion



Aerosol simulation
with EMAC

A. Pozzer et al.

Title Page

Abstract

Introduction

Conclusions

References

Tables

Figures

◀

▶

◀

▶

Back

Close

Full Screen / Esc

Printer-friendly Version

Interactive Discussion

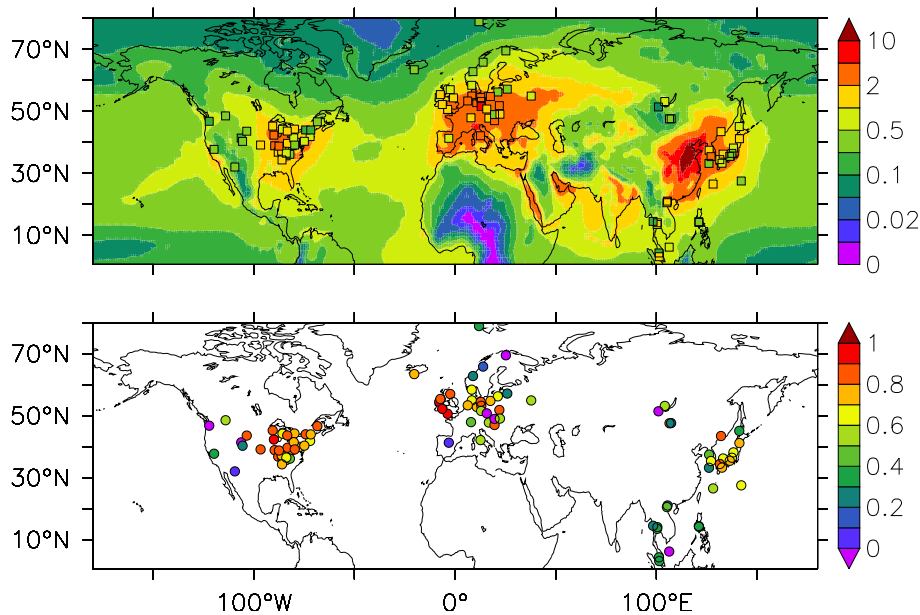


Fig. 6. As Fig. 4 but for NO_3^- .

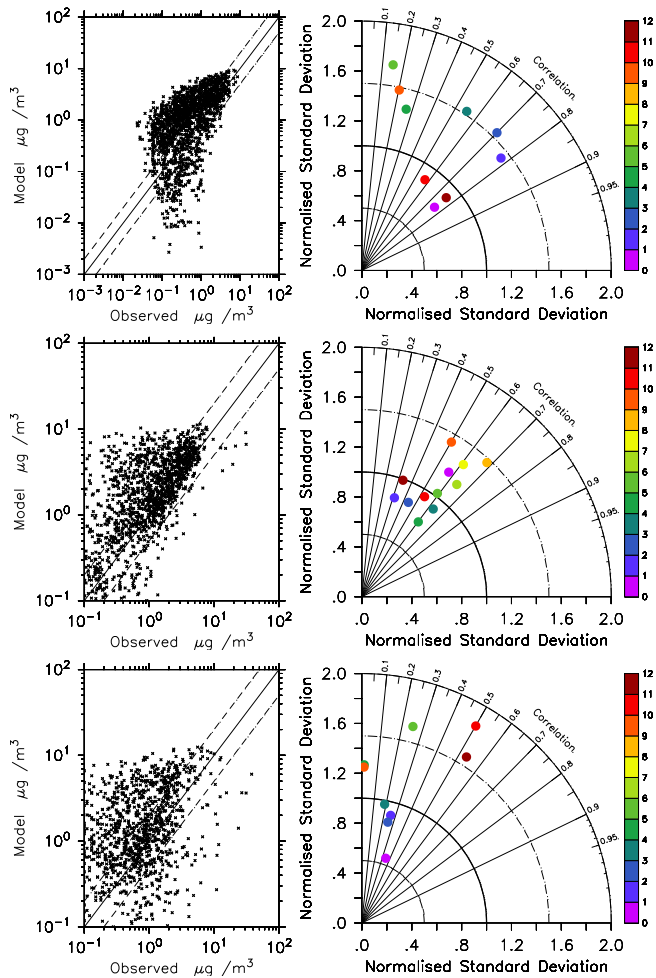


Fig. 7. As Fig. 5 but for NO_3^- .

**Aerosol simulation
with EMAC**

A. Pozzer et al.

Title Page

Abstract Introduction

Conclusions References

Tables Figures

◀ ▶

◀ ▶

Back Close

Full Screen / Esc

Printer-friendly Version

Interactive Discussion



Aerosol simulation with EMAC

A. Pozzer et al.

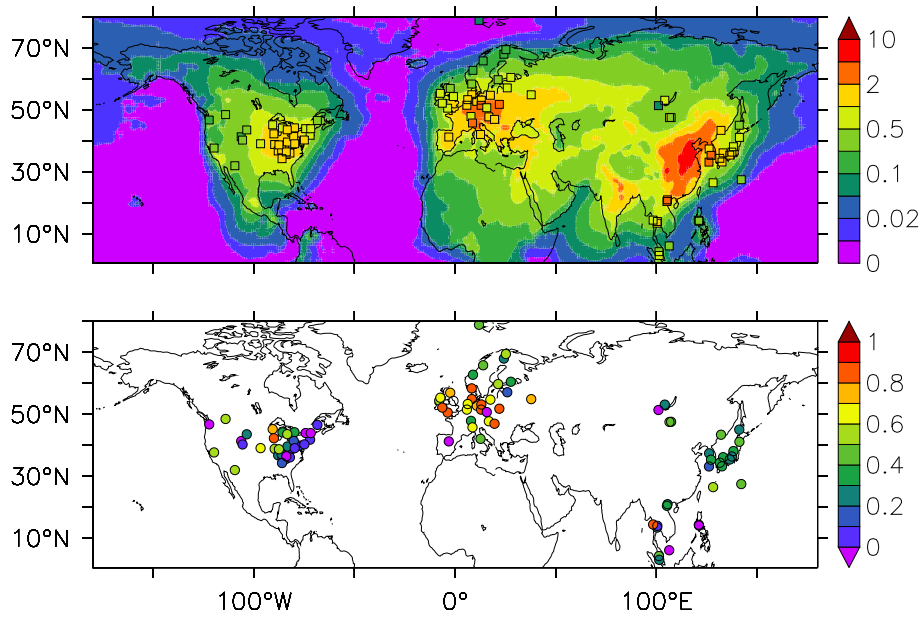


Fig. 8. As Fig. 4 but for NH_4^+ .

Title Page	
Abstract	Introduction
Conclusions	References
Tables	Figures
◀	▶
◀	▶
Back	Close
Full Screen / Esc	
Printer-friendly Version	
Interactive Discussion	



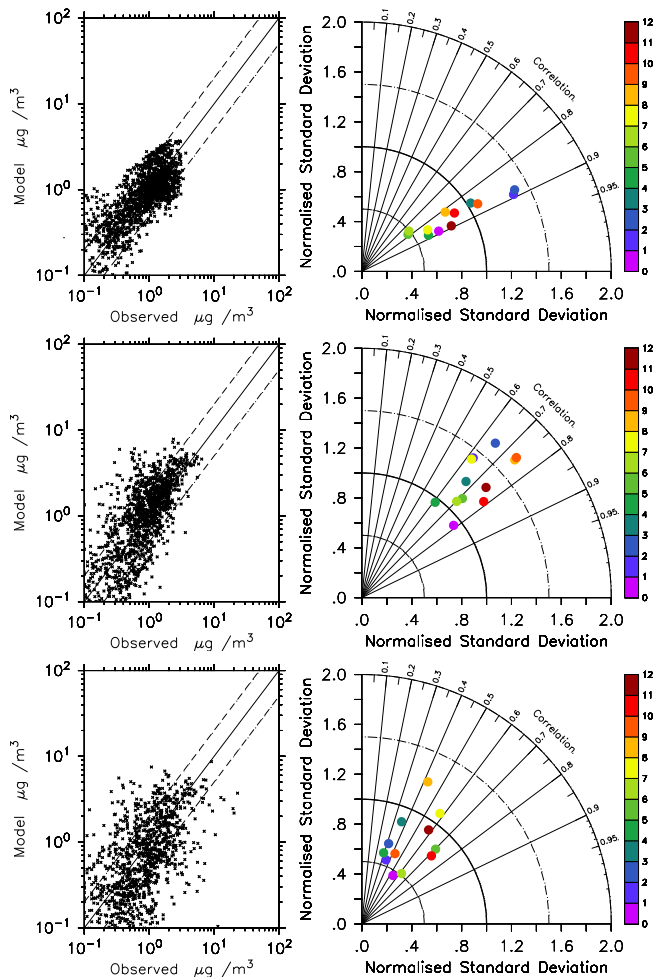


Fig. 9. As Fig. 5 but for NH_4^+ .

**Aerosol simulation
with EMAC**

A. Pozzer et al.

Title Page	
Abstract	Introduction
Conclusions	References
Tables	Figures
◀	▶
◀	▶
Back	Close
Full Screen / Esc	
Printer-friendly Version	
Interactive Discussion	



Aerosol simulation
with EMAC

A. Pozzer et al.

Title Page

Abstract

Introduction

Conclusions

References

Tables

Figures

◀

▶

◀

▶

Back

Close

Full Screen / Esc

Printer-friendly Version

Interactive Discussion

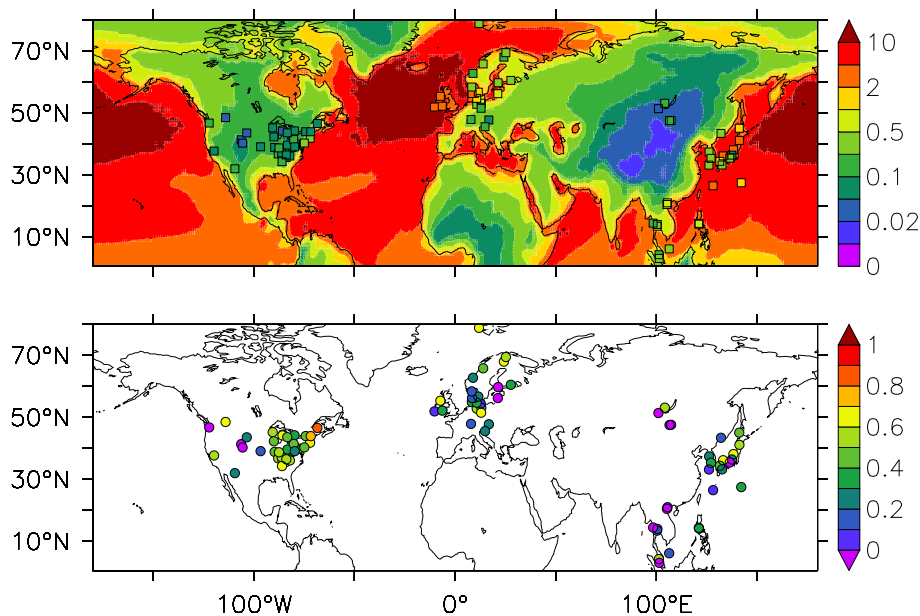


Fig. 10. As Fig. 4 but for Na^+ .

Aerosol simulation
with EMAC

A. Pozzer et al.

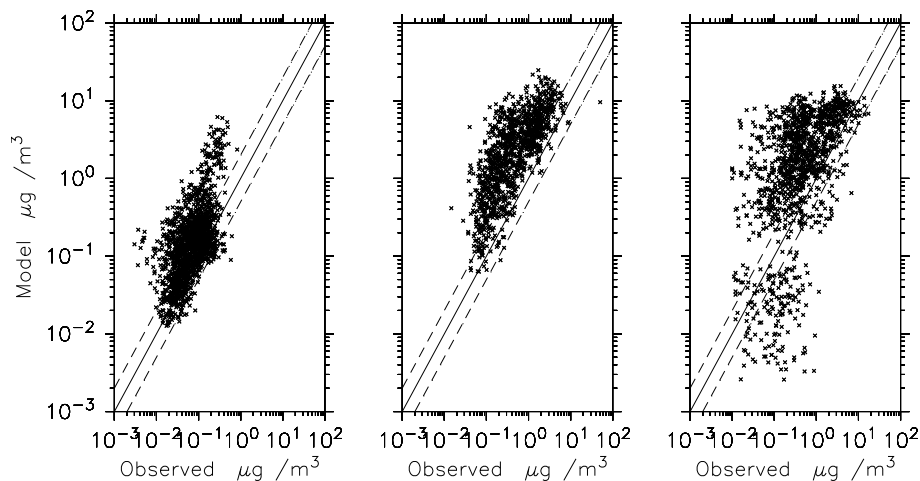


Fig. 11. Scatter plots of station observed and modelled monthly averaged concentrations (in $\mu\text{g m}^{-3}$) for the year 2005–2008 of Na^+ . LEFT: observation from CASTNET, MIDDLE: observations from EMEP, RIGHT: observations from EANET.

[Title Page](#)[Abstract](#)[Introduction](#)[Conclusions](#)[References](#)[Tables](#)[Figures](#)[◀](#)[▶](#)[◀](#)[▶](#)[Back](#)[Close](#)[Full Screen / Esc](#)[Printer-friendly Version](#)[Interactive Discussion](#)

Aerosol simulation
with EMAC

A. Pozzer et al.

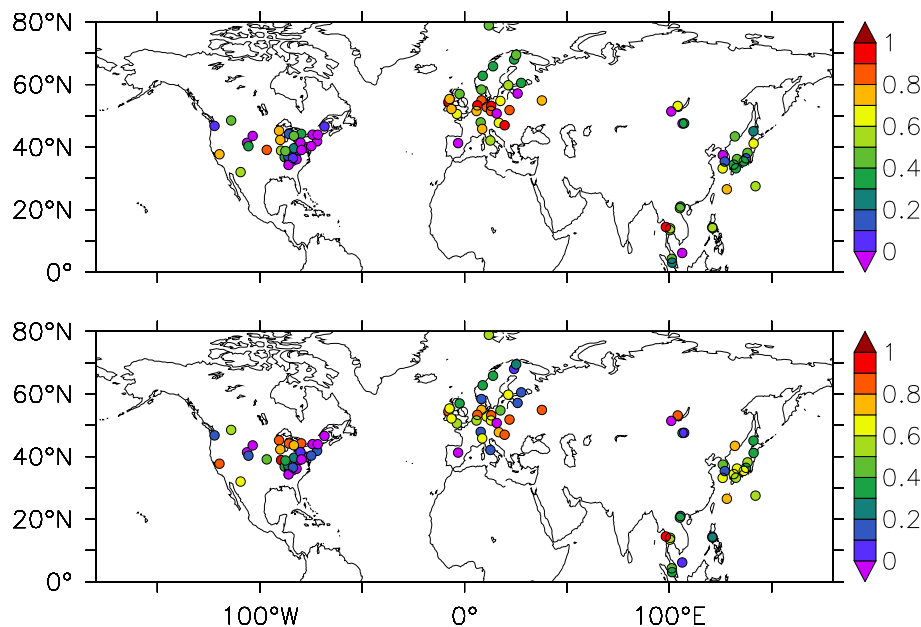


Fig. 12. Temporal correlation of observations from CASTNET, EMEP and EANET and model results for the year 2005 of NH_4^+ . UPPER: model results from simulation ST; LOWER: model results from simulation NS.

Title Page

Abstract

Introduction

Conclusions

References

Tables

Figures

◀

▶

◀

▶

Back

Close

Full Screen / Esc

Printer-friendly Version

Interactive Discussion

